UNIVERSIDADE DA BEIRA INTERIOR
Ciências

Desenvolvimento e Funcionalização de Nanopartículas de Ouro com Revestimento de Sílica para Aplicação na Terapia do Cancro

Telma Maria Andrade Jacinto

Dissertação para obtenção do Grau de Mestre em
Bioquímica
(2º ciclo de estudos)

Orientador: Professor Doutor Ilídio Joaquim Sobreira Correia
Co-orientador: Mestre André Ferreira Moreira
Mestre Ana Carolina Félix Rodrigues

Covilhã, junho de 2019

Aos meus pais, irmão, avó Maria e avó Olivia.

"Keep your eyes on the stars, and your feet on the ground."

Theodore Roosevelt

Agradecimentos

Primeiro, quero agradecer ao meu orientador Professor Ilídio Correia, por me ter deixado fazer parte do seu grupo de trabalho e provar que a exigência e a boa disposição andam sempre de mãos dadas. Estou grata pela sua orientação, recomendações e exigência, sem dúvida foram essenciais, não só para o desenvolvimento desta dissertação, mas também para o meu crescimento pessoal e profissional.

Ao meu co-orientador, André Moreira, agradeço toda a ajuda, paciência e tempo despendido comigo ao longo deste ano, sem ele a realização desta dissertação não seria possível. Estou muito grata por todo o saber que me transmitiu, pela constante disponibilidade para esclarecer dúvidas e solucionar problemas, e claro pela sua contagiante boa disposição. Não há palavras que descrevam o quão grata lhe sou!

À Carolina, quero agradecer todo o tempo despendido, toda a prontidão para me ajudar e todo o conhecimento que me transmitiu. Obrigada, por tornares esta aventura mais fácil e divertida de encarar! O meu carinho por ti é equivalente aos meus bons dias!

Aos meus colegas do grupo de investigação, gostaria de agradecer pelo seu apoio e pela constante alegria. À Rosa e ao Daniel agradeço-lhes por tornarem esta caminhada muito mais fácil de percorrer, por serem os DJs do electrospinning, por todo o apoio, pelas gargalhadas e claro pela companhia aos fim-de-semanas. À Cátia Alves, agradeço todas as palavras de incentivo, todo carinho que tem pelos seus "pikis" e as suas "skills" no illustrator. À Rita, agradeço as gargalhadas contagiantes, todo o apoio e a disponibilidade constante para ajudar. À Sónia, Duarte e Beta, um grande obrigada pelo incansável apoio e pelo excelente ambiente. Têm um lugarzinho no meu coração.

Às meninas que a Covilhã me deu, Débora, Bé, Lima, Laura e Mariana obrigada por terem tornado estes 5 anos inesquecíveis, por fazerem da Covilhã a minha segunda casa, por todas as gargalhadas, por todas as conversas, por todos os cafés prolongados e por demonstrarem que mesmo longe da vista estamos perto no coração. À minha afilhada, colega de casa e amiga, Bruna, agradeço toda a paciência para aturar os meus dilemas, todo apoio incansável, o constante otimismo e por tornar a mansão da MC a melhor casa da Covilhã.

Às minhas eternas amigas da Vila e ao Pedro, agradeço o constante apoio, incentivo e por me mostrarem que uma amizade não é feita de palavras, mas sim de atos. Obrigada por demonstrarem que apesar de estarmos em diferentes pontos do país, o laço que nos une é mais forte que qualquer distância. Que a estes longos anos e a todas as etapas que festejámos juntas se somem mais, porque isto sim será um amor para a vida toda. Um obrigada especial à Cátia, por ser amiga, companheira de estudo, pseudo-mãe, por ter estado presente presencialmente

em todas os momentos ao longo destes 5 anos e claro, por ter estado literalmente ao meu lado ao longo deste ano!

Por fim, agradeço aos meus pais, os meus eternos pilares, sou eternamente grata por todos os valores que me transmitiram, por todo o sacrifício, pela compreensão constante, por me incentivarem a ser sempre mais e melhor, a nunca desistir dos meus objetivos, e claro por todo o amor incondicional. À minha mãe, por ser a melhor do mundo, agradeço-lhe todos os conselhos, toda a confiança que deposita em mim e por ser uma eterna mãe galinha. Ao meu pai, agradeço-lhe toda a paciência, o "bullying" constante, e por ser a reflexão da minha personalidade. Ao meu irmão, por ser sempre o meu exemplo a seguir, por todo o apoio incondicional e toda a paciência que tem comigo. Por sempre ser a menina dos olhos dele, mesmo nos momentos em que o tiro do sério. À minha avó Olivia, por ser a avó babada que é, um enorme obrigada por estar sempre presente. Aos meus padrinhos, agradeço por sempre me incentivarem a lutar pelos meus objetivos e claro, por serem como segundos pais. À Filipa, agradeço-lhe por todo o carinho, palavras de incentivo e por ser como uma minha irmã.

Resumo

O cancro é uma das principais causas de morte a nível mundial, e dados recentes apontam para um aumento na incidência desta doença nos próximos anos. Por outro lado, os tratamentos convencionais tais como a cirurgia, radioterapia e quimioterapia apresentam uma baixa eficácia e toxicidade sistémica, o que tem motivado o desenvolvimento de novas terapias anticancerígenas. Nesta área, a aplicação de nanomateriais para mediar um efeito fototérmico (*i.e.* produção de calor em resposta a um estímulo de luz) e consequente morte das células cancerígenas tem sido alvo de diferentes estudos realizados por parte dos investigadores e profissionais de saúde. Entre os diversos tipos de nanopartículas desenvolvidas até ao momento, as nanopartículas de ouro revestidas com sílica mesoporosa (AuMSS) apresentam excelentes propriedades físico-químicas e biológicas, que possibilitam a sua aplicação como agentes fototérmicos e transportadores de fármacos. Contudo, a aplicação destas nanopartículas na terapia contra o cancro é dificultada pelo seu reduzido tempo de circulação na corrente sanguínea e baixa especificidade para o tecido tumoral.

As limitações destes sistemas despoletaram o desenvolvimento da presente dissertação que teve como objetivo a funcionalização de superfície das nanopartículas AuMSS com forma de bastonete com novos polímeros biofuncionais com a finalidade de aumentar o seu tempo de circulação na corrente sanguínea, a sua internalização pelas células cancerígenas, e ainda incrementar o seu efeito terapêutico. Para tal, as AuMSS em forma de bastonete foram modificadas quimicamente com diferentes rácios (1:1 e 4:1) de Succinato de D-α-tocoferol polietilenoglicol 1000 (TPGS) e Ácido Hialurónico (HA). O HA foi selecionado devido à sua especificidade para os recetores CD44 que estão sobreexpressos na membrana das células cancerígenas. Por outro lado, o TPGS devido à sua natureza anfifílica possuiu a capacidade de aumentar a solubilidade, e por consequência a estabilidade coloidal das nanopartículas, incrementando assim o seu tempo de circulação no sangue.

Os resultados obtidos demonstraram que a funcionalização dos AuMSS em forma de bastonete permitiu a neutralização da carga de superfície de -28 ± 10 mV para -3 ± 5 mV e 11 ± 2 mV, para as AuMSS-TPGS-HA (1:1) e (4:1), respetivamente, sem comprometer a distribuição de tamanhos dos nanomateriais ou a sua capacidade fototérmica. Para além disto, o sucesso da ligação dos polímeros às nanopartículas foi confirmado por espectroscopia de infravermelho por transformada de Fourier (FTIR) e análise termogravimétrica (TGA). Nos ensaios *in vitro* foi demonstrada a biocompatibilidade de todas as formulações produzidas até concentrações de 200 µg/mL, quando estas foram colocadas em contacto com células saudáveis (fibroblastos) e cancerígenas (cancro do colo do útero). Contudo, a funcionalização com TPGS e HA melhorou a hemocompatibilidade dos nanomateriais bem como a sua seletividade para as células

cancerígenas do colo do útero. Por fim, o efeito fototérmico mediado pelas AuMSS com forma de bastonete induziu eficazmente a morte das células cancerígenas.

Em suma, os resultados apresentados nesta dissertação confirmam que a funcionalização das AuMSS com os polímeros TPGS e HA foi bem-sucedida. Por outro lado, foi também demonstrado o potencial das AuMSS para serem aplicadas na terapia fototérmica do cancro.

Palavras-chave

Cancro, Nanopartículas de Ouro com Revestimento de Sílica, HA, Terapia Fototérmica, TPGS.

Resumo alargado

Na atualidade, o cancro é um dos principais problemas de saúde pública, apresentando uma incidência e mortalidade crescente na população mundial. Este cenário deve-se à baixa eficácia dos tratamentos convencionais aplicados na clínica, tais como a radioterapia, cirurgia e quimioterapia. Dentro destes tratamentos, a quimioterapia é o tratamento mais aplicado, no entanto este exibe problemas que condicionam a sua aplicação. Os agentes quimioterápicos apresentam uma baixa solubilidade, reduzida seletividade para o tecido tumoral e são rapidamente degradados, o que resulta numa baixa biodisponibilidade, reduzida eficácia terapêutica e efeitos secundários associados aos tratamentos. Por outro lado, as células cancerígenas podem adquirir um fenótipo de resistência a múltiplos fármacos, reduzindo assim a eficácia da terapêutica. Deste modo é fundamental desenvolver novas abordagens terapêuticas para o tratamento do cancro.

Nesta área, os avanços na área da nanotecnologia permitiram desenvolver sistemas à escala nanométrica (nanopartículas) capazes de superar as limitações associadas às terapias convencionais. De facto, a terapia fototérmica mediada por nanomateriais tem sido alvo de diferentes estudos realizados por investigadores e profissionais de saúde. Este tipo de abordagem terapêutica tira partido da capacidade intrínseca das nanopartículas se acumularem no tecido tumoral e produzirem calor quando irradiadas com um comprimento de onda específico. Este aumento localizado na temperatura pode promover danos irreversíveis no tecido tumoral que é irradiado, levando à sua destruição. Além disso, de forma a garantir a máxima eficácia da terapia fototérmica é essencial a utilização de luz com um comprimento de onda no infravermelho próximo (NIR, 750-1100 nm), uma vez que esta radiação apresenta uma baixa interação com os componentes do corpo humano. Esta propriedade garante assim uma maior penetração nos tecidos biológicos e consequente na ativação dos nanomateriais.

Dentro dos diferentes tipos de nanopartículas em desenvolvimento, as AuMSS com forma de bastonete têm sido muito estudadas para aplicação na área do cancro, devido às suas propriedades físico-químicas que permitem a sua aplicação não só na terapia, mas também na imagiologia. O elevado coeficiente de atenuação de raios-X e o efeito de Raman do núcleo de ouro permite a aplicação destes materiais como agentes de imagiologia. Por outro lado, o núcleo de ouro das AuMSS também tem a capacidade de converter a radiação NIR em calor, causando assim hipertermia na zona do tecido tumoral, o que pode levar a danos irreversíveis nas células cancerígenas. Por sua vez, a camada de sílica mesoporosa protege o núcleo de ouro da degradação, pode ser carregada com fármacos anticancerígenos e é facilmente funcionalizada com diferentes polímeros. No entanto, a aplicação destas nanopartículas na terapia contra o cancro é dificultada pelo seu reduzido tempo de circulação na corrente sanguínea e pela baixa especificidade para o tecido tumoral.

Na presente dissertação, desenvolveram-se nanopartículas AuMSS com forma de bastonetes, funcionalizadas na sua superfície com polímeros biofuncionais, com o objetivo de aumentar o tempo de circulação na corrente sanguínea, a sua internalização no tecido tumoral e ainda incrementar o seu efeito terapêutico. Para tal, as AuMSS em forma de bastonete foram funcionalizadas com HA e TPGS. O HA foi selecionado devido à sua afinidade com o recetor CD44, sobreexpresso pelas células cancerígenas, podendo assim funcionar como uma molécula de direcionamento ativo da nanopartícula. Por outro lado, o TPGS devido à sua natureza anfifílica tem a capacidade de aumentar a solubilidade, e por consequência a estabilidade coloidal das nanopartículas, aumentando assim o tempo de circulação sanguínea dos nanosistemas. Adicionalmente, o TPGS pode atuar como um inibidor da P-gp, uma bomba de efluxo altamente expressa nas células cancerígenas, sendo um dos mecanismos de resistência a fármacos apresentados por estas células. Desta forma a utilização deste polímero poderá levar uma diminuição do efluxo dos agentes terapêuticos e à maximização da eficácia destas nanopartículas.

As AuMSS produzidas apresentaram uma morfologia uniforme com um núcleo de ouro e um revestimento de sílica bem definidos. A modificação das AuMSS foi conseguida promovendo a condensação de diferentes rácios (1:1 e 4:1) dos polímeros TPGS e HA previamente modificados com um silano (Isocianato de 3-(trimetoxisilil) propil-TESPIC). Esta modificação resultou na neutralização da carga de superfície dos nanomateriais de -28 ± 10 mV para -3 ± 5 mV AuMSS-TPGS-HA (1:1) e 11 ± 2 mV AuMSS-TPGS-HA (4:1), sem comprometer a distribuição de tamanhos dos nanomateriais. A ligação dos polímeros à superfície das nanopartículas foi confirmada pelas técnicas FTIR e TGA. A nível da capacidade fototérmica, todas as formulações conseguiram mediar um aumento de temperatura de cerca de 20 ºC. Nos ensaios *in vitro* foi ainda demonstrada a biocompatibilidade de todas as formulações até 200 µg/mL. Adicionalmente, a funcionalização com TPGS e HA melhorou a hemocompatibilidade e aumentou a seletividade das AuMSS para as células cancerígenas do colo do útero, destacando-se a este nível a formulação AuMSS-TPGS-HA (4:1) que apresentou o menor valor de hemólise e uma menor acumulação nos fibroblastos (células saudáveis). Por fim, o efeito fototérmico mediado pelos AuMSS em forma de bastonete induziu eficazmente a morte das células cancerígenas do colo do útero.

Em suma, os resultados apresentados nesta dissertação confirmam que a modificação da superfície das AuMSS com polímeros TPGS e HA foi realizada com sucesso. Para além disso, foi também verificado o potencial das AuMSS para aplicação na terapia fototérmica direcionada do cancro.

Abstract

Cancer is one of the leading causes of death in the worldwide population and recent data indicates that its incidence will continue to increase in the next years. On the other hand, the traditional treatments such as surgery, radiotherapy, and chemotherapy have low therapeutic efficacies and induce systemic toxicity. Such have prompted the development of new therapeutic approaches for cancer. In this area, the application of nanomaterials to mediate a photothermal effect (*i.e.* heat generation upon light irradiation) and consequently induce the death of cancer cells has gained a considerable recognition by researchers and health professionals. Among the various types of nanoparticles developed until now, gold core-mesoporous silica coated nanoparticles (AuMSS) have excellent physicochemical and biological properties, which allow their application as photothermal agents and drug carriers. However, the application of these nanoparticles in cancer therapy is hindered by their reduced blood circulation time and poor specificity to the tumor tissue.

Thus, the present dissertation aimed to develop a new surface functionalization for the rod-shaped AuMSS nanoparticles based on biofunctional polymers, in order to increase its blood circulation time, internalization by the cancer cells, and ultimately increase the therapeutic effect. For this purpose, the rod-shaped AuMSS were chemically modified with different ratios (1:1 and 4:1) of D-α-Tocopherol polyethylene glycol 1000 succinate (TPGS) and Hyaluronic Acid (HA). HA was selected due to its specificity towards the CD44 receptors that are overexpressed in the cancer cells' membrane. On the other hand, TPGS owing to its amphiphilic nature is able to increase the nanomaterials solubility, and consequently its colloidal stability that enhances the blood circulation time.

The obtained results showed that the rod-shaped AuMSS' functionalization neutralized the nanoparticles' surface charge, from -28 ± 10 mV to -3 ± 5 mV and 11 ± 2 mV for AuMSS-TPGS-HA (1:1) and (4:1), respectively, without compromising the nanomaterials' size distribution or photothermal capacity. Moreover, the success of the polymers grafting to the nanoparticles was confirmed by Fourier Transform Infrared (FTIR) spectroscopy and thermogravimetric analysis (TGA). *In vitro* assays demonstrated the biocompatibility of all formulations at concentrations up to 200 µg / mL in both healthy (fibroblast) and cancerous (cervical cancer) cells. However, the functionalization with TPGS and HA has improved the nanomaterials' hemocompatibility as well as their selectivity towards cervical cancer cells. Finally, the photothermal effect mediated by the rod-shaped AuMSS effectively induced the death of the cancer cells.

In summary, the results presented in this dissertation confirm the successful functionalization of the AuMSS with the TPGS and HA. Additionally, the AuMSSs' potential to be applied in cancer photothermal therapy was also demonstrated.

Keywords

Cancer, Gold Core Silica Shell Nanoparticles, HA, Photothermal Therapy, TPGS.

List of publications

Articles in peer-reviewed international journals:

Reis CA, Rodrigues CF, Moreira AF, Jacinto TA, Ferreira P, Correia IJ. Development of gold-core silica shell nanospheres coated with poly-2-ethyl-oxazoline and ß-cyclodextrin aimed for cancer therapy. Materials Science and Engineering: C. 2019; 98:960-8 DOI: 10.2217/nnm-2018-0179

Rodrigues CF*, Jacinto TA*, Moreira AF*, Costa EC, Miguel SP, Correia IJ. Functionalization of AuMSS nanorods towards more effective cancer therapies. Nano Research. 2019;12(4):719-32. DOI: 10.1007/s12274-019-2286-y

Moreira AF, Rodrigues CF, Jacinto TA, Miguel SP, Costa EC, Correia IJ. Microneedles Mediated Chemotherapy and Photothermal Therapy for the Treatment of Cancer. *Submitted for publication.*

Jacinto TA, Rodrigues CF, Moreira AF, Miguel SP, Costa EC, Ferreira P, Correia IJ. AuMSS nanorods coated with TPGS and HA for cancer targeted photothermal therapy. *Submitted for publication.*

*These authors contributed equally to this article.

Index

Chapter I

1. Introduction 2

1.1. Cancer 2

1.1.1. Cancer epidemiology 2

1.1.2. Cancer development and hallmarks 2

1.1.3. Conventional treatments 4

1.2 Nanotechnology aimed for cancer photothermal therapy 5

1.2.1. Photothermal therapy benefits in cancer treatment 5

1.2.2. Main features of nanoparticles 6

1.2.3. Nanocarriers classes for photothermal therapy 9

1.3. AuMSS nanorods 10

1.3.1. Synthesis 10

1.3.2. Properties of AuMSS nanorods 11

1.4. AuMSS nanorods functionalization strategies 12

1.4.1. Optimizing the blood circulation time 12

1.4.2. Stimuli-responsive behavior 15

1.4.3. Tumor targeting 18

1.5 AuMSS nanorods application as cancer therapeutic agents 21

Aims 23

Chapter II

2. Materials and Methods 25

2.1. Materials 25

2.2. Methods 25

2.2.1. Synthesis of AuMSS nanorods 25

2.2.2. Removal of the surfactant template 26

2.2.3. Synthesis of TESPIC-TPGS and TESPIC-HA derivatives 26

2.2.4 AuMSS nanorods' functionalization 26

2.2.5. Characterization of nanocarriers' physicochemical properties 27

2.2.5.1. Morphological characterization and size analysis 27
2.2.5.2. Zeta potential analysis 27
2.2.5.3. Ultraviolet-visible spectroscopy analysis 27
2.2.5.4. Fourier transform infrared spectroscopy analysis 28
2.2.5.5. Thermogravimetric analysis 28
2.2.6. *In vitro* photothermal measurements 28
2.2.7. Cytocompatibility assays 28
2.2.7.1. Cell viability 28
2.2.7.2. Hemolysis 29
2.2.7.3. HeLa cells live/dead assay 29
2.2.8. Cellular uptake by HeLa and FibH cells 29
2.2.9. Characterization of the 2D cytotoxic profile of the nanoparticles 30
2.2.10. Statistical analysis 30

Chapter III

3. Results and Discussion 32
3.1. Synthesis and characterization of TESPIC-TPGS and TESPIC-HA polymers 32
3.2. Synthesis and characterization of AuMSS nanorods 34
3.3. Functionalization of the AuMSS nanorods 36
3.4. *In vitro* evaluation of the AuMSS nanorods' photothermal capacity 37
3.5. Nanoparticles biocompatibility 38
3.5.1. Cell viability 38
3.5.2. HeLa cells live/dead assay 40
3.5.3. Hemolysis 41
3.5.4. Cellular uptake by HeLa and FibH cells 42
3.5.5. Characterization of the AuMSS nanorods phototherapeutic effect 43

Chapter IV

4. Conclusion 46

Chapter V

5. References 48

Figure Index

Figure 1 - Representation of the cancer tissue heterogeneity 3
Figure 2 - Cancer cells' hallmark 4
Figure 3 - Overview of the main physicochemical properties. 8
Figure 4 – Representation of the different classes of nanoparticles 9
Figure 5 - General properties and main applications of the AuMSS nanoparticles 10
Figure 6 - Representation of the nanoparticles' functionalization 27
Figure 7 - Synthesis schematic of TESPIC-TPGS and TESPIC-HA polymers 32
Figure 8 - FTIR and NMR spectra of TPGS, TESPIC-TPGS, HA and TESPIC-HA polymers. 33
Figure 9 - AuMSS nanoformulations morphology and size distribution 35
Figure 10 - FTIR spectra of AuMSS, AuMSS-TPGS-HA (1:1) and AuMSS-TPGS-HA (4:1). 36
Figure 11- Physicochemical characterization of AuMSS formulations. 37
Figure 12 - Characterization of the AuMSS nanoformulations' *in vitro* PTT capacity 38
Figure 13 - Evaluation of AuMSS nanoformulations' cytocompatibility 39
Figure 14 - Live/Death CLSM images of HeLa cells incubated with the different AuMSS nanorods formulations 40
Figure 15 - Analysis of the AuMSS nanorods' hemocompatibility 41
Figure 16 - Representative confocal microscopy images of the AuMSS formulations uptake by HeLa cells 42
Figure 17 - Fluorescence spectroscopy analysis of uncoated and coated AuMSS nanorods uptake by FibH and HeLa cells 43
Figure 18 - Cytotoxic effect of AuMSS nanoformulations in HeLa cells 44

Abbreviations

A549	Human lung carcinoma
AA	L-ascorbic acid
ANOVA	One-way analysis of variance
AR	Aspect ratio
AS1411	Nucleolin aptamer
AuMSS	Gold core and mesoporous silica shell
AuMSS-TPGS-HA (1:1)	AuMSS-TPGS-HA with TPGS/HA ratio (1:1)
AuMSS-TPGS-HA (4:1)	AuMSS-TPGS-HA with TPGS/HA ratio (4:1)
BSA	Bovine serum albumin
CLSM	Confocal laser scanning microscopy
COS7	Fibroblast-like cell lines derived from monkey kidney tissue
CT	Computerized tomography
CTAB	Cetyltrimethylammonium bromide
DMA	Dimethylmaleic anhydride
DMEM-F12	Dulbecco's modified eagle medium/nutrient mixture F-12
DMEM-HG	Dulbecco’s modified eagle medium-high glucose
DMSO	Dimethyl sulfoxide
DNA	Deoxyribonucleic acid
Dox	Doxorubicin hydrochloride
ECM	Extracellular matrix
EDTA	Ethylenediamine tetraacetic acid
EPR	Enhanced permeability and retention
EtOH	Ethanol
FBS	Fetal bovine serum
FibH	Human fibroblasts
FITC	Fluorescein 5-isothiocyanate
FTIR	Fourier transform infrared spectroscopy
FA	Folic acid
HA	Hyaluronic acid
HeLa	Human negroid cervix epithelioid carcinoma
HepG2	Liver hepatocellular carcinoma
IgM	Imunoglobulin M
K^-	Negative control
K^+	Positive control
L02	Human hepatic cell line
MCF-7	Breast cancer cell line
MDR	Multidrug resistance
MGC803	Human gastric cancer cell line

MRI	Magnetic resonance imaging
N2a	Neuroblastoma cancer cells
NIR	Near infrared
PBS	Phosphate-buffered saline
PDT	Photodynamic therapy
PEG	Polyethylene glycol
PFA	Paraformaldehyde
P-gp	Glycoprotein-P
PTT	Phothermal therapy
RBC	Red blood cells
RES	Reticuloendothelial system
RGD	Arginylglycylaspartic acid
RVG-29	29 residue peptide derived from rabies virus glycoprotein
S2VP10L	Pancreatic adenocarcinoma cells
SCID	Severe combined immunodeficiency
TEM	Transmission electron microscopy
TEOS	Tetraethyl orthosilicate
TESPIC	3-(Triethoxysilyl)propyl isocyanate
TESPIC-HA	TESPIC modified HA
TESPIC-TPGS	TESPIC modified TPGS
TGA	Thermogravimetric analysis
THF	Tetrahydrofuran
TME	Tumor microenvironment
$TMPyP_4$	Tetrakis(4-N-methylpyridiniumyl) porphyrin
TMS	Tetramethylsilane
TPGS	D-α tocopherol polyethylene glycol 1000 succinate
U87	Human glioblastoma cells
USA	United States of America
UV-vis	Ultraviolet-visible
WGA-Alexa Fluor® 594	Wheat germ agglutinin conjugate Alexa 594®

Chapter I

Introduction

This chapter is based on the publication entitled: “Functionalization of AuMSS nanorods towards more effective cancer therapies.” Nano Research. 2019;12(4):719-32.

1. Introduction

1.1. Cancer

1.1.1. Cancer epidemiology

Cancer, due to is complexity, is the second leading cause of the worldwide population (1). The latest reports available in the literature estimate that in 2018, eighteen million of new cancer cases were diagnosed and nine million of cancer-related deaths occurred worldwide (2). In the present year, only in the United States of America (USA), it is predicted that the cancer will be responsible for more than six hundred thousand of deaths and more than one million seven hundred thousand new cancer cases will be detected (3). On the other hand, a study conducted by the *Direcção Geral de Saúde* revealed that the cancer incidence in Portugal has been increasing at a rate of 3% per year (4). Moreover, this study also reports that the cancer mortality and incidence in 2035 will be close to thirty thousand and sixty thousand cases, respectively.

In men, lung cancer is the most mortal and diagnosed cancer worldwide, followed by prostate and colorectal cancers in incidence and the stomach and liver cancers in mortality. In turn, the breast cancer is the most mortal and diagnosed cancer in women, followed by colorectal for incidence and lung for mortality (2).

As stated above, the cancer incidence and mortality have been growing worldwide and the reasons for such phenomenon are complex. Nevertheless, there are several risk factors that already have been related with increased probabilities to develop cancer, such as smoking, alcohol consumption, diet, obesity, physical inactivity, infections, ionizing and solar radiation, as well as hormones and/or genetic susceptibility (5).

1.1.2. Cancer development and hallmarks

Cancer leads to the formation of complex and heterogeneous tissues that are developed via a multistep process, involving abundant genomic and epigenomic alterations that eventually lead to the malignant transformation of a normal cell (carcinogenesis) (6). Additionally, the cancer tissue is also composed of immune and stromal cells (*e.g.* fibroblasts and endothelial cells), as well as the extracellular matrix (ECM) (*e.g.* collagen), that form the so-called tumor microenvironment (TME) (Figure 1) (7). The cross-talk between these and the cancer cells plays an important role on the cancer development and metastasis (8). In fact, the cancer cells' interaction with the TME constituents can trigger dynamic signaling circuits that promotes the cancer progression. In that way, Hanahan and Weinberg defined several key characteristics (*i.e.* hallmarks of cancer) for the cancer cells' establishment, survival, and growth (9, 10). In

this regard, the cancer cells' capacity to maintain its continuous proliferation is one of the most important cancer hallmarks (Figure 2).

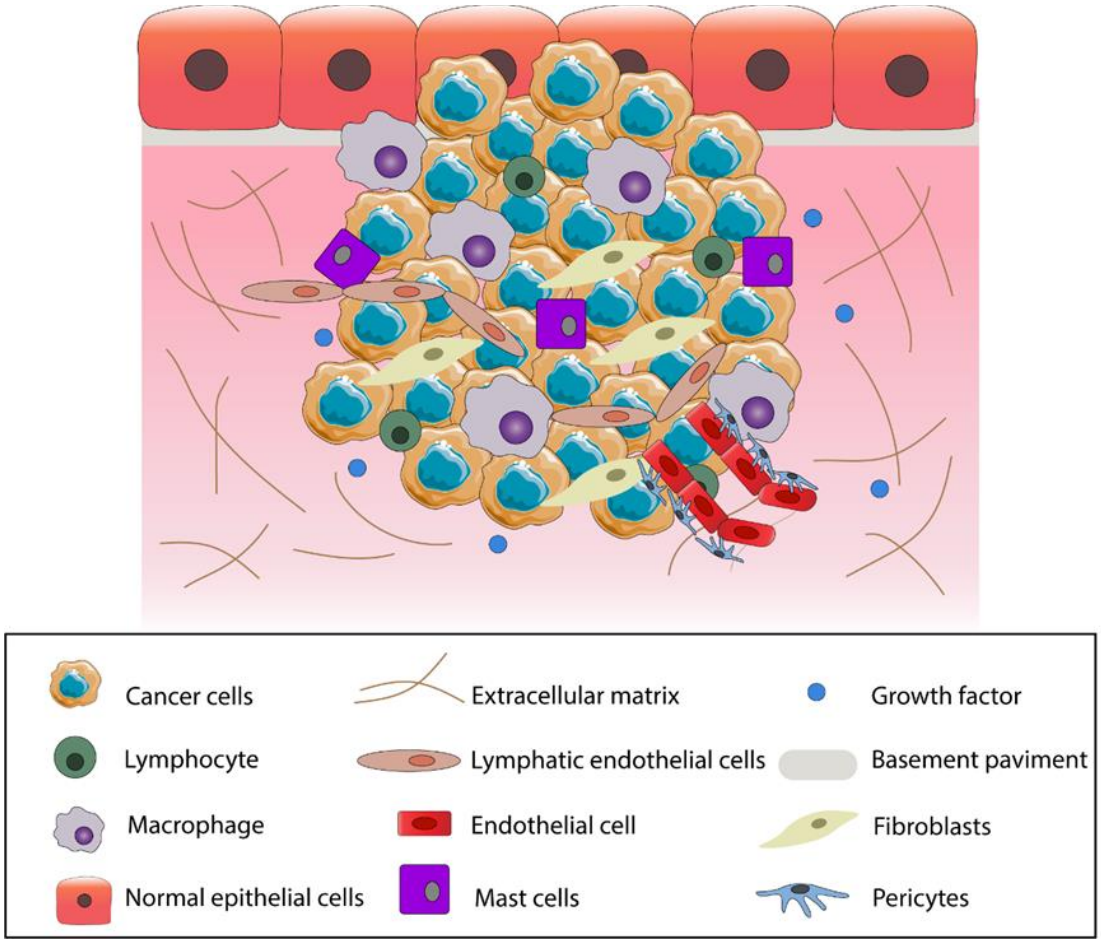

Figure 1 - Representation of the cancer tissue heterogeneity. Complex TME characterized by the cross-talking between malignant, endothelial, pericytes, fibroblasts, immune system cells, and the ECM.

Fundamentally, cancer cells can keep a proliferative state by producing themselves growth factors (*i.e.* autocrine signaling), stimulating the TME constituents to produce growth factors (*i.e.* paracrine signaling), and overexpressing the growth receptors (*i.e.* the tumor cells will be hyperresponsive to low levels of growth factors) (11). On the other hand, cancer cells also present an increased resistance to antigrowth signals, mainly those responsible for regulating the cell apoptosis. For instance, cancer cells can increase the expression of anti-apoptotic molecules (*e.g.* Bcl-2, Bcl-xL, and Bcl-w), down-regulate the pro-apoptotic proteins (*e.g.* Bax and Bak), or even avoid the action of growth suppressors (*e.g.* p53 and retinoblastoma (Rb) tumor suppressors) (12, 13). Simultaneously, the cancer cells also overexpress the telomerase, an enzyme capable of maintaining the length of telomeres by adding repeated sequences of hexanucleotides, rendering to them a limitless proliferative potential by avoiding the cell senescence (14).

To further support the cells' proliferation, the cancer cells can also induce the angiogenesis in order to facilitate the access to oxygen and nutrients as well as to allow the removal of the metabolic wastes. More recently, the cancer cells' capacity to avoid the recognition and destruction by the immune system as well as their metabolic plasticity (*e.g.* adjustments in the glycolytic pathways) were also reported as essential for the tumor proliferation and progression (10).

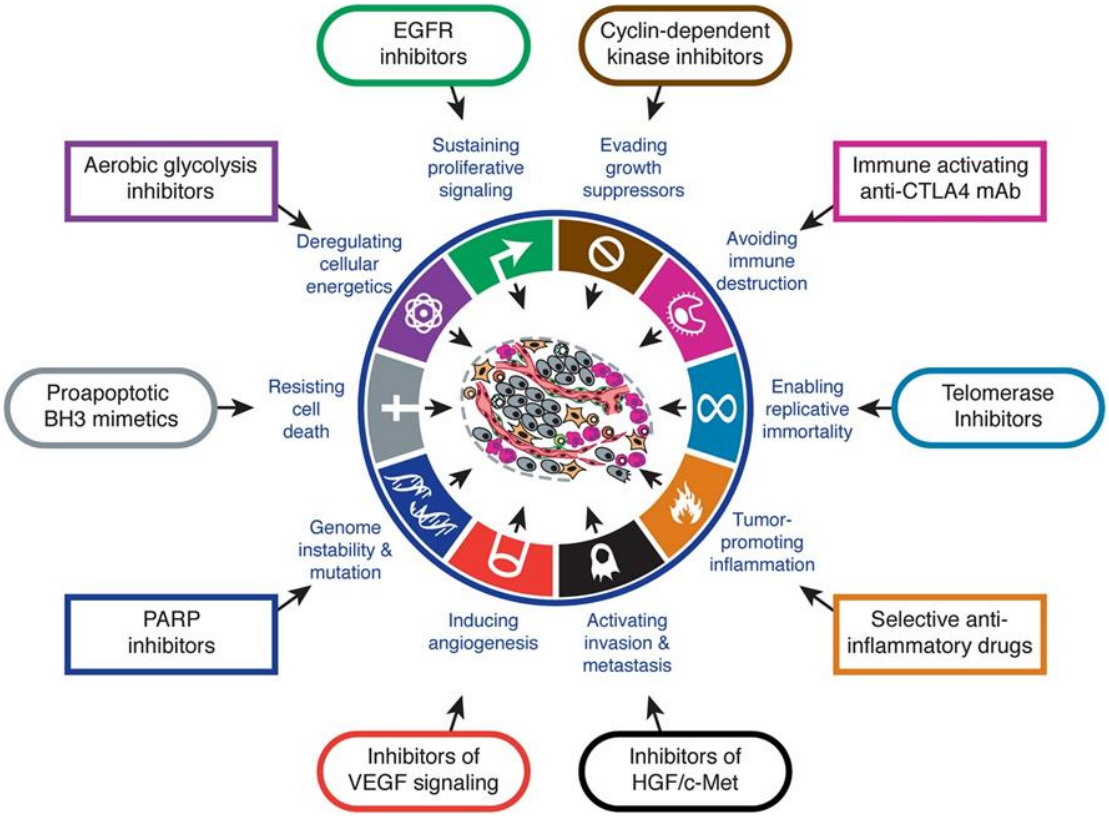

Figure 2 - Cancer cells' hallmarks and examples of the drug types that target each one of these key characteristics for tumor growth and progression (reproduced from (10)).

1.1.3. Conventional treatments

In the clinic, the most used treatments for cancer therapy are the surgery, chemotherapy, and radiotherapy (15). Particularly, a cancer patient is often subjected to a therapeutic combination, usually the surgical removal of the tumor mass followed by chemotherapy and/or radiotherapy sessions (16). Nevertheless, these therapeutic approaches present a sub-optimal efficacy and provoke several side effects that can even lead to the patient death. For example, the surgical removal of the tumor mass induces scarring, does not guarantee the complete removal of the cancer cells, and also affects the healthy tissue close to the tumor. On the other side, the radiotherapy is often related with local and systemic damage of healthy tissues. Similarly, the chemotherapy also causes several life-threatening side effects such as nausea, vomiting, fatigue, pain, increase risk of sepsis, cardiovascular toxicity, and infertility (17, 18). Further, the cancer cells may also develop resistance against radio- and chemo- therapies,

which greatly reduces their therapeutic potential (19). The cancer cells can counteract the drugs action by increasing the drug efflux by membrane transporters, reducing the drug absorption, inhibiting the apoptosis, modifying the drug metabolism and target, and enhancing the DNA damage repair. Further, the acquisition of this multi-drug resistance phenotype by cancer cells in response to a specific drug treatment also lead to the development of resistance against other chemotherapeutic agents even if they are chemically, structurally, and functionally different (20). In this way, it is pivotal to develop of new and more effective anti-cancer therapies.

1.2 Nanotechnology aimed for cancer photothermal therapy

Nanotechnology has becoming a promising vehicle not just to cancer therapy, but also for cancer detection, monitoring, and diagnosis. Additionally, the nanomedicines have the potential to minimize or even bypass the drawbacks of conventional therapies (21). In this way, the photothermal therapy (PTT) mediated by nanomaterials it is considered a noninvasive highly promising alternative for cancer therapy (22). In fact, the combination of the nanomaterials' intrinsic affinity to accumulate in the tumor tissue with the light activated therapeutic effect allows the specific targeting of the tumor cells, minimizing the damage to the surrounding healthy tissues (23).

1.2.1. Photothermal therapy benefits in cancer treatment

The PTT mediated by nanomaterials explores the utilization of near infrared radiation (NIR) (700-1000 nm) as trigger to induce the cell death. The selection of this wavelengths have as rationale to exploit the minimal light absorption and scattering in this region of the spectra by the biological components (*e.g.* water, hemoglobin, skin, and other pigments), which will increase the NIR light penetration in the human body (2-10 cm) (24, 25). Therefore, upon NIR light irradiation, the nanomaterials will convert the absorbed energy into heat. Such reaction can promote a localized temperature increase in the tumor tissue, which when reaches temperatures around 41-47 °C start to induce negative effects over the cancer cells viability and sensitizes them to the chemotherapeutics action. Additionally, further increases in the temperature (45-90 °C) will cause irreversible cellular damages, *i.e.* DNA destruction, protein denaturation, and disruption of the cellular membranes, ultimately causing cellular apoptosis (26). Until now, several nanomaterials (*e.g.* gold, palladium, graphene, and copper) have been explored to mediate this PTT. Nevertheless, to achieve the maximum potential of the nanomaterials-mediated PTT, the nanoparticles' physicochemical parameters must be carefully optimized since they have a crucial role on the nanoparticles' interaction with the human body at a cellular and molecular level. In the following section, the main nanoparticle's

characteristics (*i.e.* size, charge, shape, composition, and targeting) affecting their blood circulation, biodistribution, and ultimately tumor accumulation are discussed.

1.2.2. Main features of nanoparticles

The influence of the nanoparticles' physicochemical properties on their biological performance is closely linked to the several physiological barriers that the nanoparticles must overcome when administered in the human body.

After the intravenous administration, the nanoparticles must maintain its colloidal stability in order to avoid their degradation or aggregation (27). Further, the nanoparticles must also circumvent the rapid clearance by the renal filtration as well as the uptake and retention by the reticuloendothelial system organs. Moreover, during the blood circulation, the nanoparticles should present minimal adsorption of plasma proteins (*e.g.* serum albumin, apolipoproteins, complement components, and immunoglobulins) since the nanoparticles surface opsonization leads to the activation of phagocytes and to their clearance from circulation (28). Furthermore, nanoparticles must be also capable of extravasating from the blood vessels to the tumor tissue. This process is highly dependent on the abnormal architecture of the blood vessels and the reduced lymphatic drainage (EPR effect) of the tumor tissue (29). The tumor vasculature displays increased fenestrae' sizes ranging from 200 to 1200 nm, which facilitate the nanoparticles' extravasation to the tumor. On the other side, the impaired lymphatic drainage increases the nanoparticles' retention time on this tissue. Furthermore, recently it was also described that can occur dynamic and short-lived eruptions in the blood vessels of the tumor, allowing an increased blood flow into the tumor interstitial space and consequently the nanoparticles' extravasation (30). At the tumor site, the nanoparticles must penetrate deeply into the tumor, to reach the majority of the cancer cells. However, this can be impaired by the tumors' dense ECM and interstitial fluid pressure (31). Lastly, the final barrier that the nanomedicines must overcome is the cell membrane.

The nanoparticles' size, charge, and shape are crucial factors on their interaction with the different biological components. Moreover, the nanoparticles' surface composition (*e.g.* corona and targeting moieties) will dictate the nanoparticles' biodistribution and tumor accumulation. In the next sub-sections, the nanoparticles' fine-tuning (size, charge, shape, corona, and targeting moieties) for enhancing their blood circulation time, tumor accumulation, cellular internalization, and ultimately their anticancer efficacy will be discussed (Figure 3).

- **Size**

The size is one of the main parameters that influence the nanoparticles blood circulation and biodistribution. For instance, nanoparticles with a size inferior to 5 nm present an increased elimination through renal filtration. On the other side, sizes inferior to 50 nm facilitate the nanoparticles extravasation from the liver vasculature and therefore the accumulation in this organ. Additionally, larger sized particles (*i.e.* superior to 200 nm) are prone to be recognized by macrophages and Kupffer cells as well as entrapped in the spleen (17, 32-35). Therefore, considering the enhanced permeability and retention (EPR) effect and the size constrains for the nanoparticles' blood circulation, in the literature is often referred a size range between 100-200 nm as the ideal for cancer nanomedicines. Despite influencing the nanoparticles' biodistribution (*e.g.* tumor accumulation), the size also affects their tumor penetration and cellular uptake. In the literature, the larger nanoparticles become mostly accumulated at the tumor periphery, while the smaller nanoparticles present a faster and deeper tumor penetration (28). After reaching the cancer cells, the nanoparticles capacity to transpose the cell membrane is also size-dependent. In fact, smaller nanoparticle (4-10 nm) can be internalized in cancer cells by direct transposition of the lipid bilayer membrane (36). While, bigger nanocarriers are internalized by pinocytosis, in a process that can occur via clathrin-dependent endocytosis (nanoparticles with ~120 nm, destined to lysosomes) or clathrin-independent endocytosis. The latter pathway also encompasses the caveolin-dependent endocytosis (nanoparticles ~60 nm), clathrin-and caveolin-independent endocytosis (nanoparticles with ~120 nm), and macropinocytosis (particles >1 μm) (37, 38).

- **Charge**

The nanoparticles' surface charge is another key parameter on their design, affecting the nanoparticles' circulation time, toxicity, tumor penetration, and interaction with cancer cells. For instance, highly charged nanoparticles (*i.e.* surface charges superior to ± 10 mV) are prone to interact with the reticuloendothelial system (RES) cells and proteins during the blood circulation (39). The proteins adsorption can increase the particles' size and promote its aggregation hindering their tumor accumulation, whereas the surface opsonization favors the nanoparticles recognition by immune system cells leading to their clearance (40). Moreover, highly charged nanoparticles also present an impaired tumor penetration due to their strong interaction with the charged components of the tumor ECM (*e.g.* hyaluronic acid (HA) and collagen). Therefore, a neutral surface charge (± 10 mV) is often desirable for improving the nanoparticles blood circulation time as well as the tumor accumulation and penetration (28).

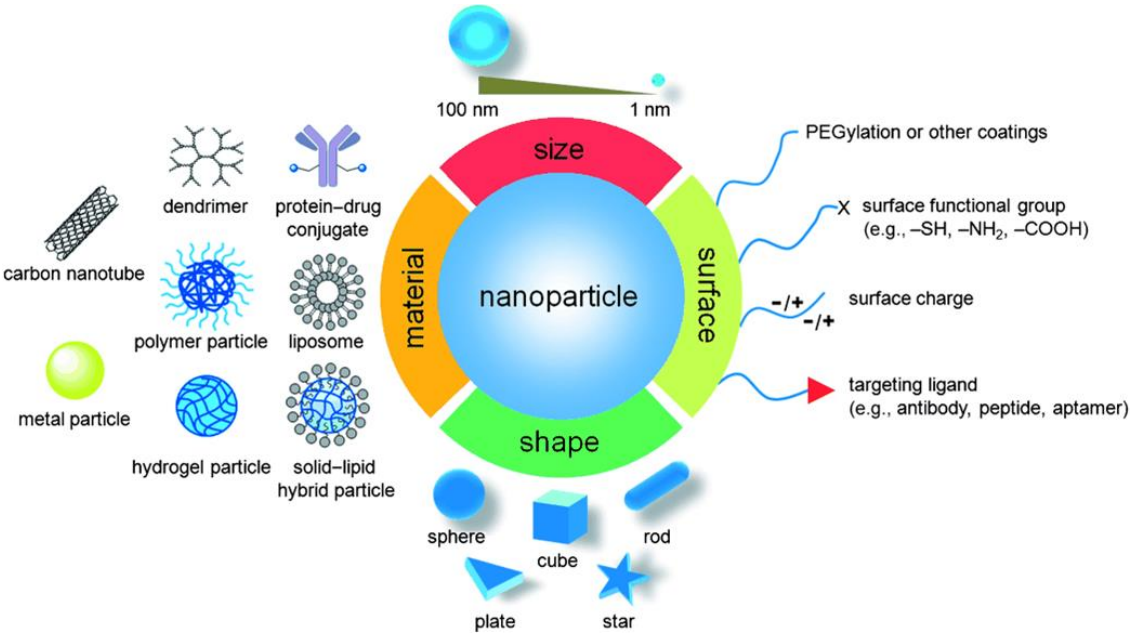

Figure 3 - Overview of the main physicochemical properties that affect the nanoparticles biological performance (reproduced from (41)).

- **Shape**

The shape can also affect the nanomaterials' interaction with the human body. Nevertheless, the real effect of the nanoparticles shape on their biological performance appears to be material dependent, and to fully understand the shape effect further studies are still required. For example, Dias and colleagues verified that rod-like AuMSS presented an increased cellular uptake in 2D cell cultures, whereas the spherical counterparts had a higher tumor penetration in 3D spheroids (42). Black and colleagues reported that the functionalization of Au nanospheres with polyethylene glycol (PEG) have a higher blood circulation time and lower RES uptake comparatively to gold nanorods, nanocages, and nanodisks. Further, the same authors also observed that the nanorods and nanocages could reach deeper regions of the tumor tissue, while the nanospheres and nanodisks remained mainly on tumor surface (43). Additionally, the nanoparticles' shape also dictates if they circulate in periphery or central region of the blood vessels. The circulation near to the blood vessels' wall is desirable for enhancing the nanoparticles' probability to extravasate into the tumor site (44). In this way, spherical nanoparticles circulate preferentially in the center of the blood vessels, whereas anisotropic particles such as nanorods present rotation and tumbling movement, which increases their lateral drift to the vessel walls, and consequently facilitates the extravasation through the tumor vessels fenestrae (45).

- **Surface Composition**

The nanoparticles' surface functionalization (*e.g.* hydrophilic polymers and red blood cells (RBC) based coatings) can improve their solubility, stability, biodistribution, and biocompatibility (46). For that purpose, the selected material usually prevents the formation of the protein corona, *i.e.* the adsorption of proteins on the nanoparticles' surface that affects nanoparticle's immunogenicity, cellular uptake, and pharmacokinetics (47, 48). Furthermore, the proteins adsorption can also induce changes on the nanoparticles' size and surface charge (49). Such events facilitate the nanoparticles' elimination through the RES or may change their safety profile (50). On the other hand, the nanoparticles can also be grafted with target ligands, such as HA, arginylglycylaspartic acid (RGD), and folic acid (FA) (51, 52). These molecules explore the host-guest, antibody-antigen, and ligand-receptor interactions to increase the nanoparticles' selectivity towards the tumor tissue.

1.2.3. Nanocarriers classes for photothermal therapy

The nanomedicines can be divided in two major categories, organic and inorganic. Within these classes, there are nanomaterials that present intrinsic properties compatible with PTT-related applications (53). One of the deciding factors is the material capacity to absorb NIR light and convert it into heat. Therefore, carbon nanotubes, gold nanoparticles, and graphene oxide sheets arise as some of the most explored NIR-light responsive nanomaterials for mediating the cancer PTT (Figure 4) (54).

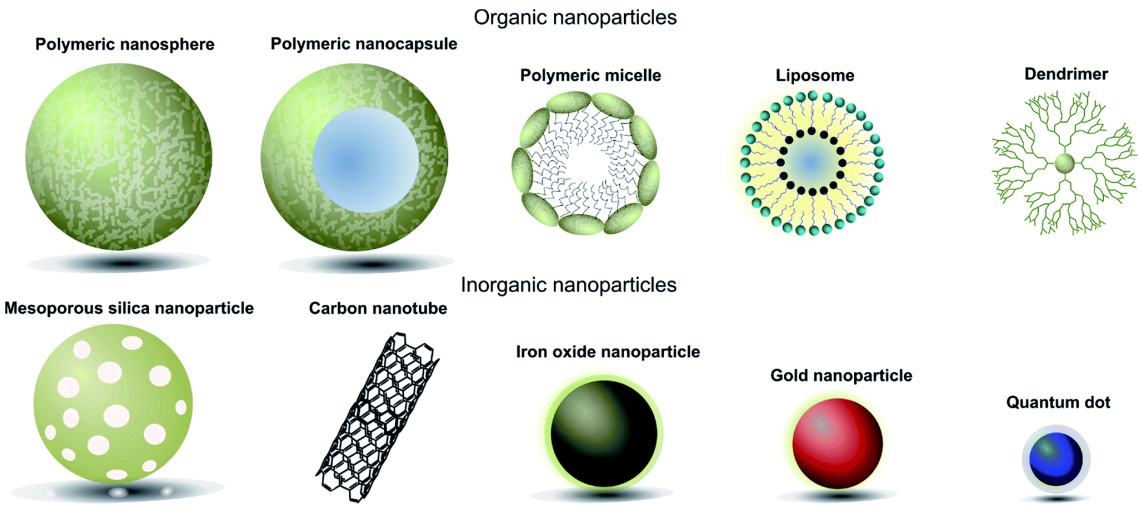

Figure 4 – Representation of the different classes of nanoparticles (Reproduced from (55)).

Among these, gold nanoparticles have been widely applied in PTT due to their good physical and optical properties. The optical properties of gold nanoparticles are based on the surface plasmon resonance phenomenon, which makes them capable of absorbing and/or scattering light (56). Additionally, the gold nanoparticles shape versatility allows the fine-tuning of its

plasmonic resonance wavelength from 520 nm to the NIR region of the spectrum (24). Within them, the anisotropic gold nanostructures and particularly the gold nanorods have been extensively explored for cancer PTT. Nevertheless, the gold nanoparticles reshaping phenomena (degradation) when exposed to high-energy radiations and its affinity to interact with thiol groups (*i.e.* non-specific binding with biomolecules) hinders the gold nanoparticles application in biological systems (52).

The surface coating is one of the solutions explored to address the gold nanoparticles limitations and simultaneously potentiate its application in cancer therapy. From the wide number of materials tested so far, the gold-core silica shell (AuMSS) nanoparticles are a promising route to prepare multifunctional anti-cancer nanomedicines. In the next sections, it is provided a general overview of the AuMSS nanorods synthesis procedure, main properties, and application in cancer therapy (Figure 5). Additionally, the AuMSS nanorods surface modifications aimed to enhance its blood circulation time, increase tumor accumulation and control the drugs release are also described.

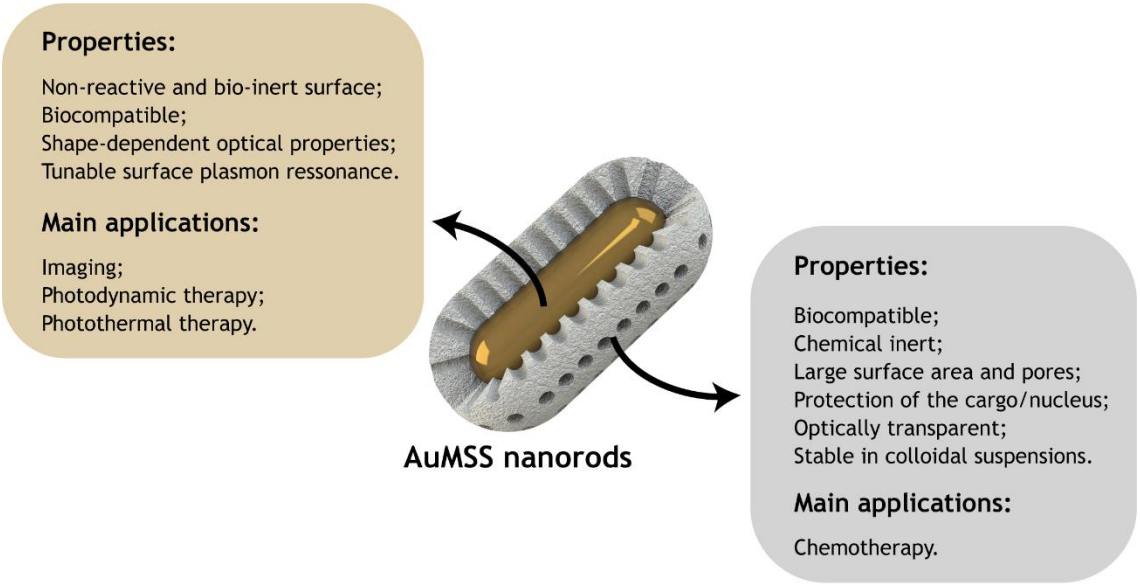

Figure 5 - General properties and main applications of the AuMSS nanoparticles.

1.3. AuMSS nanorods

1.3.1. Synthesis

The synthesis of AuMSS can be divided in two main steps, the production of the gold nucleus followed by the coating with a mesoporous silica shell (42). For this purpose, different techniques have been used to produce gold nanorods such as seed-mediated growth, electrochemical, template-assisted, photochemical, and lithographic methods (57). Between them, the seed-mediated growth is one of the most used due to its simplicity, scalability, and

efficiency (57, 58). This process relies on the utilization of small seed particles of gold that are grown to display a final nanorod morphology. Briefly, the seed nanoparticles are generated under conditions of high chemical supersaturation in the presence of a strong reducing agent (*e.g.* $NaBH_4$), which promotes the uniform gold nucleation in small spherical nuclei (*i.e.* 1 to 5 nm) (59, 60). Subsequently, the gold seeds are added to a "growth" solution containing a gold salt, cetyltrimethylammonium bromide, a reducing agent (*e.g.* ascorbic acid) and silver nitrate to induce the gold nucleation with a rod-shaped growth (60). During this reaction, cetyltrimethylammonium bromide acts simultaneously both as stabilizer and as a template agent (61). The silver nitrate allows the fine-tuning of the gold nanorod aspect ratio (AR), due to the preferential formation of AgBr complexes on the {110} gold facets (62). Such allows the other facets (*i.e.* {111} and {100}) of the gold nucleus to grow faster originating the gold nanorods (62). In fact, in the literature, it is reported that an increase in the concentration of silver ions, when maintaining the amount of seeds constant, leads to a red-shift on the longitudinal plasmon band of the gold nanorods (58). Similarly, the gold nanorods AR (*i.e.* length/width quotient) can also be optimized by adjusting the initial amount of the seed solution (60). Pérez-Juste and colleagues observed that in the presence of fixed values of silver ions, the increase in the amount of seeds resulted in an increase of the gold nanorods AR and consequently in a red-shift in the longitudinal plasmon band (63). Afterward, the gold nanorod is coated with a mesoporous silica shell using derivations of the Stöber method (64). In a common approach, the silica precursor (*e.g.* tetraethyl orthosilicate) will start to condensate at the surface of the gold nanorod in a base catalyzed reaction using cetyltrimethylammonium bromide micelles as pore structuring agents (65). Such is mediated by the electrostatic interactions between the positively charged cetyltrimethylammonium bromide micelles and the negatively charged silica species (64, 65). Therefore, the thickness of the silica shell can be tailored by fine-tuning the reaction time and the reagent concentrations.

1.3.2. Properties of AuMSS nanorods

The AuMSS nanorods have been widely explored for possible cancer therapy applications due to its tunable optical properties, drug delivery potential, and effective light-heat conversion (66, 67). In fact, the gold nanomaterials have been described as biocompatible, bioinert and present a high flexibility in terms of shape, size, and surface chemistry (59). Further, the increased mass attenuation of the gold core allows the nanorods application as contrast agents on computerized tomography (CT), magnetic resonance imaging (MRI), and diffusion reflection-based imaging (68-71). On the other side, when the gold is irradiated with electromagnetic radiation at specific wavelengths, occur a collective oscillation of electrons (*i.e.* localized surface plasmon resonance) on the gold nanoparticle surface that can result in strong extinction of light (*i.e.* absorption and scattering) (72). In gold nanorods, the electron oscillations occur in two different orientations (short and long axis of the structure), creating two distinct absorption bands in the spectrum with different intensities (73). The band resulting from

oscillation along the short axis presents its peak around 500 to 600 nm (73). On the other hand, the oscillation along the long axis induces a stronger absorption band, called longitudinal band that can be tailored to the NIR region of the electromagnetic spectrum by controlling the nanorod AR (73). This absorption in the NIR region is explored to create a PTT effect that can be used to induce cellular damage (42, 74). Additionally, the inclusion of a mesoporous silica coating provides a biocompatible and chemically inert shell with a large surface area that is optically transparent to NIR light (65, 75). Moreover, the inclusion of the mesoporous silica shell stabilizes and protects the gold-core from degradation when exposed to NIR radiation and further improves the particle ability to encapsulate and deliver bioactive molecules, specifically cancer cells (76, 77). Nevertheless, the clinical application of these systems is widely constrained by the premature drug leakage from the nanoparticles and by the low blood circulation times. For that purpose, researches have been performing different surface functionalization's that are aimed for improving the AuMSS nanorods blood circulation time, drug release profile and specificity towards cancer cells, which are described in the following sections.

1.4. AuMSS nanorods functionalization strategies

1.4.1. Optimizing the blood circulation time

When biological applications are intended, the nanoparticles stability in biological fluids (*e.g.* blood and interstitial fluid) is one of the most important parameters that will affect the nanoparticles performance (78, 79). In fact, previous studies already demonstrated that when the particles are in contact with the biological media, different biomolecules (*e.g.* proteins) can adhere to the nanoparticle surface and thus influence its toxicity, cellular uptake, pharmacokinetics, and immunogenicity (80, 81). This process originates a more or less tightly adhered layer of proteins that can prompt changes on the original surface charge of the nanoparticles (cationic to anionic or vice-versa) and even promote the particles aggregation or elimination from the systemic circulation by the RES (82, 83). The composition of the nanoparticles protein corona is dynamic and dependent on the concentration and affinity of many proteins present in the blood (*e.g.* albumin, apoliproteins, C3 complement, and others) (82, 83). Therefore, researchers have been exploring the functionalization of nanoparticles with antifouling molecules to prevent proteins adsorption, which can enhance the AuMSS nanorods circulation time and consequently its accumulation in the tumor tissue (84, 85). In the literature, the PEG is one of the most explored materials for achieving this nanoparticles' "stealthing" effect. In fact, different nanoparticle-based antitumoral therapies already applied in the clinic, such as *Doxil*®, *DaunoXome*®, and *Myocet*®, have been using PEG to improve its pharmacokinetic profile. PEG is a hydrophilic and non-toxic polymer capable of reducing protein adhesion, molecular recognition, as well as non-specific cellular uptake (86, 87). This so-called

stealthing effect is generally attributed to the high level of hydration of the PEG hydrophilic polyether backbone, which originates a steric repulsion that prevents the protein adsorption in hydrophobic regions of the polymer (88-90). Nevertheless, it is worth to notice that the PEG molecular weight and surface density may impact on nanoparticles stability and biological performance. In the literature, it has often been referred that the utilization of PEG with a molecular weight (Mw) of 2000 Da or even superior results in an enhanced inhibition of the protein adsorption and nanoparticle recognition by the mononuclear phagocytic system (91, 92). Further, the density of the PEG grafting in the nanoparticle surface will affect its structural conformation. In this way, lower PEG densities in the nanoparticle surface results in a polymer mushroom-like conformation (92, 93). On the other side, an increased PEG density results in an overlap of the polymer chains that translates into a more stretched brush-like organization, which is associated with an improved ability to avoid the nanoparticles recognition and protein adsorption (80, 91, 94).

Shen and colleagues produced a doxorubicin (Dox) loaded AuMSS nanorods functionalized with PEG containing the RGD peptide in the terminal groups for improving the nanoparticles antitumoral effect (95). The AuMSS functionalization was achieved by reacting the N-Hydroxysuccinimide group in a bifunctional PEG (Mw: 3500 Da) derivative with the amine groups previously immobilized on the particle surface. The authors observed that the nanoparticles functionalization resulted in an increase in the hydrodynamic diameter from 118.6 nm to 143.9 nm. Further, the AuMSS nanorods PEGylation prevented its aggregation even when stored in water for 24 h. Moreover, in the *in vivo* assays, the authors observed that the PEGylated AuMSS nanorods did not elicit any inflammatory reactions, presenting the RBC, hematocrit, mean corpuscular volume, white blood cell, hemoglobin, and platelet parameters similar to the control, as well as reduced the Dox cardiotoxicity (95). In a similar approach, Wang *et al*. studied the pharmacokinetics and biodistribution of PEGylated AuMSS (96). For that purpose, maleimide functionalized PEG (Mw: 2000 Da) was reacted with thiol modified AuMSS nanorods. The authors observed that the inclusion of the PEG coating resulted in nanorods with a hydrodynamic diameter of 41.8 nm and induced the neutralization of the particle surface charge from negative (-14.1 mV when coated with bovine serum albumin (BSA)) to almost zero (-0.06 mV). Further, in the pharmacokinetics studies, the PEGylated AuMSS nanorods presented an enhanced blood circulation times and slower elimination rates, elimination half-life ($t_{1/2\beta}$)=6.32 h, when compared to nanorods coated with bovine serum albumin, $t_{1/2\beta}$=0.75 h. Moreover, the biodistribution studies revealed that all the nanoparticle formulations were mainly accumulated in the liver and spleen (*i.e.* liver 70-75% and spleen 5-11% of the injected dose at 24 h) without eliciting any significative toxic effects. Nevertheless, the PEGylated nanorods presented a superior accumulation in the tumor tissue (0.83% of the injected dose at 24 h) than the BSA coated counterparts (0.61% in the tumor at 24 h). On the other side, Liu and colleagues produced AuMSS nanorods coated with ß-cyclodextrin, RLA peptide (sequence: $[KLAKLAK]_2$) and PEG (Mw: 2000 Da) modified with chitosan for the enhanced photodynamic

(PDT) and PTT therapy of breast cancer (97). For this purpose, AuMSS nanorods were reacted with 3-aminopropyltriethoxysilane to introduce amine groups on the particle surface, allowing the cyclodextrin immobilization via carbodiimide chemistry.

Subsequently, methoxyPEG and carboxymethyl chitosan were chemically linked using 1-ethyl-3-(3 dimethylaminopropyl)carbodiimide/N-Hydroxysuccinimide chemistry and modified with 2,3-dimethylmaleic anhydride (DMA). The final PEG-chitosan-DMA polymer created a protective coating in the surface of cyclodextrin modified AuMSS nanorods via electrostatic interactions. Such resulted in a particle with a rod-like morphology and surface charge of -9.4 mV that could be reversed when incubated in acidic microenvironments, such as those of tumors. In fact, the authors observed that the AuMSS-β-cyclodextrin-RLA/PEG-chitosan-DMA nanoparticles suffered a surface charge reversal from -9.4 mV to 15 mV after only 3 h of incubation in pH 6.8. This behavior directly affects the protein adsorption on the nanoparticles surface, the PEGylated nanoparticles presented 16% of bovine serum albumin adsorbed after 2 h of incubation at pH 7.4, contrasting with the 68% recorded in the non-PEGylated ones. Further, at pH 6.8 both formulations presented more than 60% of protein adsorbed. Moreover, the authors also observed that the coated nanorods presented an enhanced tumor accumulation, which was attributed to the nanoparticles site-specific surface charge and the PEG antifouling properties.

Despite the promising results displayed by PEGylated nanomedicines, recently different studies have been reporting that the administration of PEG coated nanoparticles in animal models leads to a faster clearance in subsequent doses, a phenomenon called “accelerated blood clearance” (98, 99). In fact, it is suggested that the human body produces anti-PEG immunoglobulin M (IgM) antibodies that activate the complement system and prompt the nanoparticles’ clearance (99). Therefore, the researchers have been studying the development of alternative coatings that can also increase the nanoparticles blood circulation time. In this field, poly-2-oxazolines arise as one of the most promising alternatives for promoting the nanoparticles stealthing. The poly-2-oxazolines present a backbone similar to the natural peptides and are nonionic, biocompatible, highly soluble in water, and thermally stable (100). Further, this polymer reduces the unspecific interactions with serum proteins (*e.g.* albumin), opsonins and complement system mediators, minimizing the nanoparticles recognition by the RES and consequently increasing the blood circulation time (101, 102). With that in mind, Moreira and coworkers reported the production of AuMSS nanorods coated with poly-2-ethyl-2-oxazolines for the chemo- and PTT treatment of cervical cancer (103). For that purpose, the authors reacted 3-(triethoxysilyl)propyl isocyanate (TESPIC) with the poly-2-ethyl-2-oxazolines (Mw: 5000 Da) to create a silane derivative that was grafted on the particle surface in a condensation reaction. The resulting nanoparticles presented a total length of 84 nm and width of 56 nm. Further, the authors observed that the inclusion of the poly-2-ethyl-2-oxazolines on the particle surface resulted in the neutralization of the surface charge from -30 to -15 mV. Moreover, the

authors also observed a protective effect of the poly-2-ethyl-2-oxazolines, improved the nanoparticles biocompatibility namely by decreasing the RBCs lysis.

1.4.2. Stimuli-responsive behavior

One of the main challenges during the development of AuMSS nanorods for cancer chemotherapy is to confer them the capacity to control the drug release profile, in order to promote its specific accumulation at the target cell or tissue. To accomplish this objective, researchers have been developing stimuli responsive nanocarriers that only allow the drug release in the presence of specific triggers such as pH, temperature, enzymatic, electromagnetic field, NIR radiation, redox potential, ultrasound, and ATP (104-106). Considering the AuMSS structural organization, the main approaches pursuit so far to promote a stimuli-responsive drug delivery have been exploring the blocking of the silica mesopores (*i.e.* the main drug reservoirs of AuMSS) by coating the particle surface or utilizing pore capping agents. Then, the drug release will occur due to the material destruction, conformational changes or destruction of labile/cleavable bonds upon exposition to a specific stimulus.

In this field, temperature responsive materials are one of the most explored due to the intrinsic capacity of the AuMSS nanorods to produce heat in response to the nanoparticle irradiation with NIR light. Tan *et al.* reported the development of AuMSS nanorods functionalized with a pore blocking agent, 4-sulfonatocalix[4]arene, for the temperature responsive drug delivery (107). The authors produced AuMSS nanorods (silica thickness: 13.6 nm; and gold core: 46.5 nm of length and 12.9 nm of width) modified with silane-based quaternary ammonium salt stalks for allowing the complexation of 4-sulfonatocalix[4]arene via host-guest interactions. In the drug release assays, the authors observed that the rhodamine diffusion from the AuMSS could be mediated by the NIR laser irradiation. In fact, the rhodamine release increased from 10%, in the absence of irradiation, to 95% under laser irradiation (39.5 W/cm^2). Further, this system allowed a pulsatile release profile that is characterized by fast drug releases under laser irradiation followed by a slow and sustained release in the absence of the stimuli. Liu and colleagues also used a pore gatekeeper, 1-tetradecanol, for the thermoresponsive Dox delivery to KB cancer cells (108). For that purpose, after the Dox loading on the AuMSS nanorods, the particles were mixed with 1-tetradecanol, recovered by centrifugation, and dispersed in ice-cold water, allowing the gatekeeper loading on the pore opening through a phase change (*i.e.* liquid to solid). The authors observed that the resulting nanoparticles presented a 4.6 wt.% of 1-tetradecanol, which could limit or even avoid the Dox release (<5%) when the nanoparticles were incubated at 25 °C and 37 °C, for 48 h. On the other side, the incubation at 45 °C (*i.e.* temperature above the 1-tetradecanol melting point) resulted in a pronounced drug release, achieving a value close to 70% after 48 h. Further, this nanocarrier can promote the drug release upon laser irradiation and inhibit the Dox diffusion once the irradiation is switched off, reaching ≈20% of Dox released after four irradiation cycles (802 nm, 1 W/cm^2, and 10 min). In turn, Tang

and colleagues produced poly(N-isopropylacrylamide-co-N-hydroxymethyl acrylamide) coated AuMSS nanorods to accomplish a stimuli-responsive delivery of Dox to U87 glioma cells (109). In this approach, AuMSS nanorods were modified with 3-(trimethoxylsilyl) propyl methacrylate and then reacted with N-isopropylacrylamide and N-hydroxymethyl acrylamide at 75 °C. The authors observed that the functionalization with the poly(N-isopropylacrylamide-co-N-hydroxymethyl acrylamide) was 37 wt.% of the AuMSS nanorods and could mediate the Dox release in response to the nanorods NIR irradiation and consequent heat generation. Moreover, the authors confirmed that the poly(N-isopropylacrylamide-co-N-hydroxymethyl acrylamide) coating suffered conformational changes with the temperature increase from 20 °C to 60 °C, which was demonstrated by the changes on the AuMSS hydrodynamic diameter and absorbance intensity at 400 nm. On the other hand, the authors reported that in the initial 60 min, the Dox release increased from less than 5% at 37 °C, to more than 35% at 43 °C. Further, after 24 h at 43 °C around 63% of Dox was released, contrasting with the 10% at 37°C. Such behavior indicates that the AuMSS modified with poly(N-isopropylacrylamide-co-N-hydroxymethyl acrylamide) have a thermo/NIR sensitive therapeutic efficacy.

Alternatively, the pH variations that the nanoparticles can encounter when reaching the tumor tissue can also be explored to trigger the drug release. In fact, the tumor microenvironment presents a pH more acidic than that found in the blood stream or normal tissues (17, 110, 111). This acidic tumor microenvironment is related with the low blood perfusion into the tumor tissue, which leads to a decreased oxygen content and consequently favors the lactic acid production via anaerobic glycolysis (112). Therefore, materials that can respond to the pH gradient from the blood (7.4) to tumor microenvironment (5.5-6.5) have been explored to mediate the drug release from the AuMSS. Zhang *et al*. produced a pH responsive AuMSS to deliver Dox to cervical cancer cells (113). For that purpose, the Dox molecules were chemically linked to the mesoporous silica through Schiff base bonding. The AuMSS presented a gold nanorod with an average length and width of 38 nm and 8.5 nm, respectively, and a silica shell of 16 nm. Further, the authors observed that the nanoparticles hydrodynamic diameter increased from 79.2 to 113.2 nm with the Dox grafting on the nanoparticle surface. In the drug release assays, the authors demonstrated that the direct linkage of Dox to the silica shell through an acid-labile bound could prevent the drug release at pH 7.4. However, ≈70% of the Dox was released from the nanoparticles in 96 h when incubated at pH 5, a fact justified by the hydrolysis of the -C=N- Schiff base linker. Moreover, the authors also observed that the AuMSS zeta potential was pH dependent due to the Dox removal, 4.52 mV at pH 7.4 and -8.52 mV at pH 5. On the other side, Zeiderman and colleagues explored the AuMSS functionalization with chitosan to promote a pH-sensitive drug release for the therapy of pancreatic cancer (114). The authors functionalized the AuMSS nanorods via a condensation reaction with the 3-glycidyloxypropyltrimethoxysilane modified chitosan polymer. The produced AuMSS presented a mean diameter of 102 nm and a surface charge of 0.89 mV. Further, the authors observed that the chitosan functionalization could prevent the drug release (less than 10%) when the

AuMSS were incubated at pH 7.4 for 8 h. On the other side, the incubation at acidic pH (6.0 or 6.5) resulted in a faster release kinetics, around 89% of drug released after 8 h. Such is attributed to the protonation of the chitosan chains that facilitates the gemcitabine diffusion through the polymeric coating.

The redox-triggered drug release has also been widely studied for attaining nanomedicines with a tumor specific drug delivery. These strategies take advantage of the increased glutathione concentration in the tumor, 100-1000 times higher than that found in the extracellular fluids, to trigger the drug release from the nanoparticle (17). Zhang and coworkers proposed the utilization of silver nanoparticles as redox responsive pore caps of AuMSS nanorods, mediating the 5, 10, 15, 20-tetrakis(4-N-methylpyridiniumyl) porphyrin ($TMPyP_4$) delivery to cervical cancer cells (115). In this approach, the authors functionalized the AuMSS with 3-aminopropyltriethoxysilane and then reacted it with succinic anhydride to produce carboxylated AuMSS. Afterward, a 25 nucleotides Ag^+-specific single-stranded DNA scaffold was introduced in the particle surface via carbodiimide chemistry, acting as a template for the formation of the silver nanoparticles that blocked the AuMSS pores. In the drug release assays, the silver nanoparticles *in-situ* formation prevented the drug leakage (less than 4% of $TMPyP_4$ released in 10 h) when the nanoparticles were incubated with 50% human serum. However, the authors observed that the addition of 5 mM of glutathione could trigger the drug release, reaching the maximum cumulative $TMPyP_4$ release of 41%, which was even more prominent with the increase of the glutathione concentration to 10 mM (≈100% of drug released in 10 h). Moreover, the authors also demonstrated that the addition of glutathione induces an increase in the singlet oxygen signal, which corroborates the redox responsive release of $TMPyP_4$ from AuMSS nanorods. In addition, researchers have also been exploring the combination of the nanoparticle response to multiple stimuli, in order to increase the spatiotemporal control over the drug release. In this way, Zhang and *et al*. developed poly(N-isopropylacrylamide) coated AuMSS nanorods for the stimuli-sensitive drug delivery to breast cancer cells (116). The authors used 3-(methacryloxy) propyl triethoxysilane modified AuMSS nanorods to mediate the copolymerization of N-isopropylacrylamide, acrylic acids and N,N′-methylenebis(acrylamide), rendering AuMSS nanorods coated with a "doughnut" shaped polymeric shell. The authors observed that the AuMSS presented a mean size of 280 nm and a polymer shell thickness of 70 nm, which was dependent on the temperature and pH. This dual-responsive behavior was attributed to the poly(N-isopropylacrylamide) thermo-dependent phase transition and to the protonation of the acrylic acids content at lower pHs. Therefore, when comparing to the drug release at pH 7.4, the authors recorded a ≈1.5 times faster Dox release from the nanoparticles irradiated with the NIR laser (temperature raised to 48 ºC), which was further increased (>2 times faster) when combined with the incubation in the tumor-like acidic media. Similarly, Baek and colleagues also developed a pH and temperature sensitive nanosystem based on poly(N-isopropylacrylamide)-co-N-butyl imidazolium coated AuMSS nanorods for the Dox delivery to cervical cancer cells (117). The AuMSS nanorods functionalization occurred via

electrostatic interactions between the silica silanol groups and the amine groups on poly(N-isopropylacrylamide)-co-N-butyl imidazolium. The resulting AuMSS presented a hydrodynamic diameter of 220 nm and 33% of polymer content. In the drug release experiments, the authors observed that the temperature responsive behavior of poly(N-isopropylacrylamide) resulted in a NIR dependent drug release profile. Indeed, in the absence of laser irradiation, only 11% of the drug was released, which increases to 25% when the nanoparticles are irradiated (850 nm and 100 mW) for 5 min. Further, the authors demonstrated that the Dox release could be further stimulated with the combination between the NIR radiation and incubation in pH 5, reaching a Dox release of 49%. Alternatively, An and coworkers reported the development of dual-sensitive AuMSS nanorods based on a Se-Se pore gate for the Dox and indocyanine green delivery to liver and cervical cancer cells (118). For this purpose, the authors produced a diselenide linker (OH-Se-Se-OH) that was reacted with TESPIC creating a silane derivative. Then, the AuMSS nanorods were functionalized with the diselenide linker through a condensation process. This diselenide linker can be broken in redox environments and in the presence of radical oxygen species, originating Se-H groups with negative charge. Therefore, the drug release assays demonstrated that the drug release occurs in a glutathione concentration dependent manner, *i.e.* 10, 62.99, 83.03 and 91% of Dox released at 24 h with 0, 5, 10 and 20 mM of glutathione, respectively. Moreover, the nanoparticles irradiation (808 nm, 2 min with 30 min intervals) and consequent generation of radical oxygen species by indocyanine green could also trigger the Dox release, 5, 25, 35, and 37.5% of Dox released after irradiation with NIR laser 1 W/cm^2, 2 W/cm^2, and 3 W/cm^2. Further, the authors also observed that the AuMSS suffered changes in the surface charge when exposed to glutathione or laser irradiation (from 5.70 mV to -1.52 mV and -0.52 mV, respectively), due to the cleavage of Se-Se bonds and formation of negative Se-H groups.

1.4.3. Tumor targeting

Despite all the advances in the nanotherapeutic approaches, the effectiveness of the treatment will always be directly related to the nanoparticles ability to specifically target and accumulate in the tumor tissue, while affecting as few healthy cells as possible. In fact, nanoparticles present the innate ability to passively accumulate in the tumor tissue by taking advantage of the defective vasculature in this region (119, 120). The increased rate of cellular proliferation in most of the tumors results in irregular and leaky blood vessels (*i.e.* large endothelial pores with sizes ranging from 10 to 1000 nm in diameter) and in the absence of functional lymphatic vessels (119). Therefore, the nanoparticles extravasation from the blood circulation to the tumor interstitial space is facilitated and the lack of functional lymphatic vessels contributes to nanocarrier entrapment and retention in this tissue, an effect known as EPR (121, 122). Alternatively, this passive accumulation of the nanoparticles on the tumor tissue can also be explained by the occurrence of transient eruptions on the tumor blood vessels that allow the blood flow to the tumor interstitial space (120). On the other side, nanoparticles can also

contain targeting moieties that exploit ligand-receptor, antigen-antibody, and other forms of molecular recognition with molecules exclusively expressed or overexpressed in the tumor tissue (28, 123, 124). This enhanced specificity towards vascular, stromal or cancer cells that constitute the tumor microenvironment can increase the nanoparticles uptake rate and consequently improve the therapeutic outcome.

Huang and colleagues produced FA targeted AuMSS nanorods for the treatment of gastric cancer (125). The FA receptor is overexpressed in the majority of the epithelial cancers (*e.g.* ovarian, cervical, breast, and lung), which increases the probability of the nanoparticles recognition and consequent accumulation in this tissue. In their approach, the FA was linked to amine modified AuMSS nanorods via carbodiimide chemistry. The authors observed that the FA targeted AuMSS nanorods were able to accumulate in MGC803 cells presenting an intense homogeneous cytoplasmic nanoparticle staining around the nucleus after 2 h of incubation. Further, the cells incubated with non-targeted AuMSS or previously treated with free FA did not exhibit the nanoparticles staining after 30 min of incubation, whereas the FA targeted AuMSS presented abundant golden dots on the surface of the cells. Additionally, the intravenous administration of FA targeted AuMSS nanorods in nude mice bearing gastric cancer xenograft revealed that the nanoparticles could accumulate efficiently in the tumor tissue. In fact, the authors verified that occurred an increase in the contrast of the tumor tissue computed tomography images, whereas no obvious alterations were detected on the non-tumor tissues. In a similar approach, Liu and coworkers functionalized the AuMSS nanorods with FA to increase the nanoparticles specificity to KB cancer cells (108). In this way, the FA was directly grafted in the AuMSS carboxylated surface via carbodiimide chemistry. The *in vitro* targeting studies revealed that the nanorods functionalization with FA significantly increased its uptake in KB cancer cells, 14.3 pg/cell and 0.15 pg/cell for FA targeted AuMSS or PEGylated AuMSS, respectively. Further, the authors confirmed that this enhanced nanoparticle internalization was mediated by the FA receptor since the targeted AuMSS nanorods cellular uptake decreased to 7.1 pg/cell in the presence of a receptor competitor (free folate).

On the other side, Luo *et al.* reported the development of lactobionic acid modified AuMSS nanorods for the targeting of liver cancer (126). The lactobionic acid is a disaccharide composed of gluconic acid and galactose that is recognized by the asialoglycoprotein receptors, which are highly expressed by liver cancer cells. For that purpose, the authors promoted the conversion of lactobionic acid to lactobionolactone, which was reacted with 1-adamantanamine rendering the adamantine-modified lactobionic acid. Then, the AuMSS nanorods previously functionalized with ß-cyclodextrins were modified with the targeting agent exploring the host-guest interactions between ß-cyclodextrins and adamantine. The authors evaluated the nanoparticles targeting ability in both HepG2 (lactobionic acid receptor positive cells) and COS7 cells (lactobionic acid receptor negative cells), revealing that the HepG2 cells presented a 2.8 and 4 times higher fluorescence than the COS7 cells at 4 and 8 h of incubation, respectively.

Further, the authors observed that in the presence of free lactobionic acid the AuMSS uptake by HepG2 cells was reduced in a great extent. Moreover, the authors also demonstrated that the intravenous administration of lactobionic acid-modified AuMSS nanorods in tumor bearing mice result in a preferential accumulation in the tumor tissues, exhibiting a peak at 6 h after administration. Further, these targeted nanorods also mediated a temperature increase in the tumor tissue superior to that registered for the non-targeted AuMSS (53.1 °C and 45.2 °C, respectively), indicating an enhanced accumulation in the tumor tissue mediated by the lactobionic acid.

In addition, researchers have also been exploring the utilization of small peptides and oligonucleotides for increasing the AuMSS nanorods selectivity towards the cancer cells. Zhang and coworkers reported the functionalization of AuMSS nanorods with the Nucleolin aptamer AS1411 (AS1411) for targeting cervical cancer cells (115). The AS1411 is a 26-mer G-rich DNA oligonucleotide that forms G-quadruplex structures and presents high affinity to nucleolin, which is overexpressed in the cancer cells surface. In this way, the authors immobilized a thiolated AS1411 aptamer on the surface of silver nanoparticles previously grown on the pore openings of the AuMSS nanorods. The authors observed that AS1411 containing AuMSS presented a superior internalization in cervical cancer cells (nucleolin overexpressing HeLa cells) than the nanorods modified with a random DNA sequence. Nevertheless, no significant differences in the cellular internalization were observed between the nanoparticles, when incubated with L02 cells (healthy hepatocytes). In turn, Zeiderman and colleagues explored the functionalization of AuMSS nanorods with the 7 pHLIP peptide for targeting the pancreatic cancer (114). The pHLIP peptides allow the nanoparticles targeting to acidic tumors since when in low-pH environments, the protonation of Asp or Glu residues increases the peptide hydrophobicity and consequently the affinity to the membrane lipidic bilayer (127). The AuMSS nanorods were functionalized with the pHLIP peptide using succinimidyl 4-(N-maleimidomethyl)cyclohexane-1-carboxylate, which allowed the crosslinking between the amine groups of chitosan previously grafted on the AuMSS and sulfhydryl groups in the peptide. In fact, the authors observed that the targeted AuMSS nanorods incubation with S2VP10L cancer cells at pH 6.5 resulted in a 25 times higher nanoparticles internalization when compared to the cells treated at pH 7.4. Further, the uptake of the targeted system at pH 6.5 was 3 times superior to that recorded for the chitosan only functionalized AuMSS nanorods. Additionally, the authors also demonstrated that pHLIP targeting significantly improved the AuMSS nanorods accumulation in the tumor tissues of SCID mice with orthotopic pancreatic adenocarcinoma tumors, *i.e.* 24.4 times increase in the multispectral optoacoustic tomography signal for pHLIP targeted AuMSS nanorods when compared to non-targeted group.

1.5 AuMSS nanorods application as cancer therapeutic agents

The AuMSS nanorods are the most explored AuMSS-based nanoparticles when therapeutic applications are intended due to its potential to mediate PTT, PDT, chemotherapy, or their combination. In fact, the AuMSS nanorods capacity to generate heat in response to radiation in the NIR region allows them to act as mediators in PTT. This therapeutic approach aims to induce damages or even the death of cancer cells through the utilization of temperatures superior to 39.5 °C (66). Moreover, the application of NIR radiation to trigger the nanomedicines action is of paramount importance since it allows to promote an on-demand therapeutic effect with high precision and safety due to the limited or inexistent interaction between NIR radiation and the body components (biological window) (128). Huang *et al.* reported the application of FA targeted AuMSS nanorods for the PTT of gastric cancer (125). The produced nanoparticles presented a gold core with 45.97 nm in length and 17.8 nm in width coated by a mesoporous silica shell with 8.16 nm. Further, this FA targeted AuMSS nanorods presented an absorption peak in the 732 nm, which is compatible with the nanoparticles application in PTT. The *in vitro* evaluation of the PTT efficacy showed that the FA targeted AuMSS could induce the MGC803 gastric cancer cells death in the region irradiated with the NIR laser (808 nm, 4 W/cm^2 and 3 min), whereas the non-irradiated cells remained viable. Similarly, Xia and coworkers developed AuMSS nanorods enriched with CdSe/ZnS quantum dots and functionalized with FA for the PTT of cervical cancer cells (129). The AuMSS nanorods presented a gold core with 60.21 nm in length and 16.81 nm in width enclosed in a mesoporous silica shell with 12 nm of thickness, which translated in absorbance peak at 835 nm. In the *in vitro* assays, the authors observed that the AuMSS nanorods could mediate a PTT effect since after irradiation (810 nm and 3.2 W/cm^2) for 4 min the cells within the laser spot were killed, whereas the non-irradiated cells remained viable. On the other side, Lee and colleagues described the application of RVG-29 modified AuMSS nanorods for the PTT treatment of brain gliomas (130). In this study, the AuMSS nanorods were comprised by a gold core with 79.9 nm in length and 20.1 nm in width enclosed on a mesoporous silica shell with 14 nm, originating an intense absorption band on 820 nm. Such allowed the nanoparticles to mediate the increase in the solution temperature to 50 °C when irradiated for 5 min (808 nm and 1.5 W/cm^2). Further, the authors observed that the RVG-29 modified AuMSS nanorods (0.08 mM) to N2a cancer cells in conjugation with the NIR irradiation resulted in cell viability values inferior to 20%, whereas in the absence of irradiation more than 80% of cells remained viable. Additionally, during *in vivo* experiments in N2a tumor-bearing mice, the administration of RVG-29 modified AuMSS nanorods (2.5 mM, 200 µL) could suppress the tumor growth (tumor volume 124.8 mm^3) upon NIR irradiation (808 nm, 1.5 W/cm^2, and 5 min), contrasting to the 2323.2 mm^3 obtained in the control saline group at 7 days after treatment.

However, the PTT effect mediated by the AuMSS nanorods NIR irradiation can be affected by light scattering and absorption phenomena that occur when the laser travels through the human

tissues (128). Therefore, cancer cells can receive a suboptimal laser irradiation hampering the AuMSS nanorods therapeutic effect and allowing the survival and proliferation of the tumor cells (66). In this way, several researchers have been exploring the combination of the AuMSS nanorods innate capacity to mediate a PTT effect with chemotherapy or PDT approaches to enhance the therapeutic effect towards the cancer cells (105, 131). With that in mind, Shen and coworkers explored the combination of PTT and chemotherapy with RGD-PEG functionalized AuMSS nanorods for the treatment of cervical cancer (95). These nanodevices presented a gold core (length of 51.6 nm and a width of 13.2 nm) enclosed in a mesoporous silica shell with 25 nm in thickness, and an absorption peak at 840 nm. Additionally, the authors observed that the administration of AuMSS to A549 tumor-bearing mice (25 mg of nanoparticles per mice kg) could mediate a temperature increase in the tumor region to 65.9 °C after laser irradiation (808 nm and 3 W/cm^2) for 30 sec. Further, the authors also demonstrated that the standalone PTT could inhibit the tumor growth in 45.2%. Nevertheless, the combinatorial therapy provided by the AuMSS nanorods presented a superior therapeutic effectiveness, inhibiting the tumor growth in 66.5%. In a similar approach, Monem *et al*. described the application of Dox loaded PEGylated AuMSS nanorods for the combinatorial PTT and chemotherapeutic treatment of breast cancer (132). The AuMSS nanoparticles presented a strong absorption at 840 nm resulting from the gold core with 40 nm of length and 10 nm of width (13 nm mesoporous silica shell). Their results revealed that the PEGylated AuMSS nanorods could mediate an elevation on the tumor temperature in about 14 °C upon irradiation with NIR laser. Further, the combined action of the Dox and the PTT effect obtained from the AuMSS (1.7 mg of AuMSS per mice kg) inhibited the tumor growth for a period of 5 days and slowing it for the remaining 18 days, contrasting with the continuous grow observed in other test groups. Alternatively, Liu and colleagues explored the combination of PDT and PTT in breast cancer mediated by ß-cyclodextrin, chitosan, RLA peptide functionalized AuMSS nanorods loaded with indocyanine green (97). The authors observed that the AuMSS presented a gold core with 57.3 nm of length and 16.2 nm of width, a mesoporous silica shell with 21 nm, and a strong absorption peak at 813 nm. Such allowed the nanoparticles to mediate a 31.2 °C increase in the solution temperature upon irradiation with a NIR laser for 5 min (808 nm and 2 W/cm^2). The same stimuli also prompted the radical oxygen species generation via the indocyanine green loaded in the AuMSS. Moreover, the authors observed that the functionalized AuMSS nanorods (20 mg of nanoparticles per mice kg) could induce a temperature increase in the tumors of MCF-7-bearing mice to 44.91 °C when irradiated 10 min (808 nm and 1.5 W/cm^2). Further, the combination of the PTT effect with the radical oxygen species generation presented the smallest tumor volume (inferior to 100 mm^3), whereas in the standalone therapies only a small inhibition was observed (tumor volumes superior to 200 mm^3).

Aims

The main goal of this dissertation workplan was to design and develop a novel AuMSS surface modification based on biofunctional polymers to promote an active targeting to cancer cells, overcome the limited blood circulation, and ultimately potentiate the cancer PTT. To accomplish that, different ratios of the polymers D-α tocopherol polyethylene glycol 1000 succinate (TPGS) and Hyaluronic acid (HA) were used to functionalize the AuMSS nanoparticles with a rod-like shape, originating the AuMSS-TPGS-HA (1:1 or 4:1) formulations.

The specific aims of this dissertation were:

- → Synthesize, purify, and characterize the AuMSS nanorods;
- → Synthesize the TESPIC-TPGS and TESPIC-HA polymers;
- → Functionalize the AuMSS and characterize the nanoparticles' physicochemical properties;
- → Determine the AuMSS formulations photothermal capacity;
- → Evaluate the AuMSS formulations cytocompatibility and hemocompatibility;
- → Characterize the nanoparticles' cellular uptake;
- → Evaluate the PTT mediated by the nanoparticles in cervical cancer cells.

Chapter II

Materials and Methods

2. Materials and Methods

2.1. Materials

Hydrogen tetrachloroaurate (III) hydrate ($HAuCl_4$) was purchased from Alfa Aesar (Karlsruhe, Germany). Tetraethylorthosilicate (TEOS) and tetrahydrofuran (THF) were obtained from Acros Organics (Geel, Belgium). Hexadecyltrimethylammonium bromide (CTAB) was acquired from Tokyo Chemical Industry (Tokyo, Japan). Hydrochloric acid (HCl) was bought to Panreac (Barcelona, Spain). Methanol were acquired from Fisher Scientific (Oeiras, Portugal) (Carnaxide, Portugal). Sodium Hydroxide (NaOH) was purchased from Labkem (Barcelona, Spain). Dulbecco's Modified Eagle medium-high glucose (DMEM-HG), Dulbecco's Modified Eagle Medium/Nutrient Mixture F-12 (DMEM-F12), Ethanol (EtOH), Fluorescein 5-isothiocyanate (FITC), L-ascorbic acid (AA), Paraformaldehyde (PFA), Phosphate-buffered saline (PBS) solution, Resazurin, Silver nitrate ($AgNO_3$), Sodium borohydride ($NaBH_4$), D-α-tocopherol polyethylene glycol succinate (TPGS) (Mw: 1513 Da), Trypsin, 3-(Triethoxysilyl)propyl isocyanate (TESPIC), Dimethyl sulfoxide (DMSO), Tetramethylsilane (TMS), deuterated water and Ethylenediaminetetraacetic acid (EDTA) were provided by Sigma-Aldrich (Sintra, Portugal). Hyaluronic acid (HA) (Mw: 8000-15000 Da) was purchased from Carbosynth (Berkshire, UK). Hoechst 33342®, calcein acetozxmethyl (calcein AM), propidium iodide, and wheat germ agglutinin conjugate Alexa 594® (WGA-Alexa® Fluor 594) were obtained from Invitrogen (Carlsbad, CA). Human negroid cervix epithelioidcarcinoma (HeLa cells) (ATCCs CCL-2™) were acquired from ATCC (Middlesex, United Kingdom (UK)). Primary normal human dermal fibroblast (FibH) cells were bought from Promocell (Heidelberg, Germany). Fetal bovine serum (FBS) was acquired to Biochrom AG (Berlin, Germany). Cell imaging plates were purchased from Ibidi GmbH (Ibidi, Munich, Germany). Cell culture t-flasks were supplied by Orange Scientific (Braine-l'Alleud, Belgium). Double deionized and filtered water (ultrapure water) was obtained by using a Milli-Q Advantage A10 Ultrapure Water Purification System (0.22 μm filtered; 18.2 MΩ/cm at 25 °C)

2.2. Methods

2.2.1. Synthesis of AuMSS nanorods

The AuMSS nanorods were synthesized through a three-phase method, as previously described in the literature (42, 58, 133). In the first phase, a seed solution was prepared by adding, under stirring, 0.60 mL of $NaBH_4$ (0.01 M) to an aqueous solution containing 5.00 mL of CTAB (0.20 M) and 5.00 mL of $HAuCl_4$ (0.0005 M). The seed solution was left undisturbed for 6 h at 30 ºC, and then a growth solution was prepared by adding under stirring 0.21 mL of AA (0.08 M) to an

aqueous solution containing 15.00 mL of CTAB (0.20 M), 0.03 mL of $AgNO_3$ (0.10 M), and 0.30 mL of $HAuCl_4$ (0.05 M). Lastly, the previously prepared seed solution was added to the growth solution and left at 30 °C for 16 h, to obtain the gold nanorods.

The synthesis of the mesoporous silica shell was performed by adapting the method described by Dias and colleagues (42). Firstly, AuMSS nanorods were centrifuged to remove the excess of CTAB and resuspended in ultrapure water. Next, CTAB (0.01 M) was added and left under stirring overnight. Afterward, NaOH (0.10 M) was added to the solution and mixed for 30 min. Then, 0.03 mL of a solution of TEOS (20% v/v) in methanol were injected. This step was repeated three times with 30 min intervals, and the solution was left under stirring for 24 h. The final solution was centrifuged at 12 000g for 20 min and washed several times with ultrapure water to recover the AuMSS nanorods.

2.2.2. Removal of the surfactant template

The highly cytotoxic CTAB surfactant template was removed from nanoparticles by adapting a solvent based approach, already described by Moreira and co-workers (134). Briefly, the nanoparticles were resuspended in a HCl solution (7.5% v/v in EtOH), sonicated for 3 min and centrifuged (18 000g for 15 min at 4 ºC). This step was repeated several times and was followed by two additional washing steps with EtOH (99,9% v/v) and other two with ultrapure water, to completely remove the CTAB residues. The final product was recovered by centrifugation (18 000g for 15 min) and resuspended in ultrapure water.

2.2.3. Synthesis of TESPIC-TPGS and TESPIC-HA derivatives

TPGS and HA were modified with TESPIC, to allow their chemical coupling to the AuMSS nanorods surface, through a method previously described by Rodrigues and co-workers (135). Briefly, TPGS (500 mg) or HA (100 mg) were dissolved in 20 mL of anhydrous THF and left at room temperature under a nitrogen atmosphere and magnetic stirring for 6 h. Afterwards, TESPIC was added to the reaction, in a molar ratio of 1:1 for TPGS and 1:2 for HA and left under stirring for 24 h. Subsequently, the product was recovered by evaporation (Rotavap®R-215, Büchi, Switzerland) and the remaining film was hydrated with ultrapure water, sonicated, and freeze-dried. The successful production of the polymer silanated derivatives was assessed by using the Fourier transform infrared (FTIR) spectroscopy and proton nuclear magnetic resonance (1H NMR).

2.2.4 AuMSS nanorods' functionalization

The surface of AuMSS nanorods was functionalized with TESPIC-TPGS and TPGS-HA polymers by adapting a method previously described in the literature (136) (Figure 6). For that purpose, the AuMSS nanorods (20 mg) were resuspended in 40 mL of EtOH (33%, pH 4) and sonicated for

5 min. Then, TESPIC-TPGS and TESPIC-HA polymers were added to the nanoparticles' solution (TPGS/HA ratio 1:1 or 4:1 in w/w) and left under stirring at 600 rpm for 24 h. Afterward, the final solution was centrifuged (8 000g, for 25 min at 25 ºC) and washed several times with ultrapure water to recover and remove the unlinked polymer chains from the AuMSS-TPGS-HA (1:1) and (4:1) formulations.

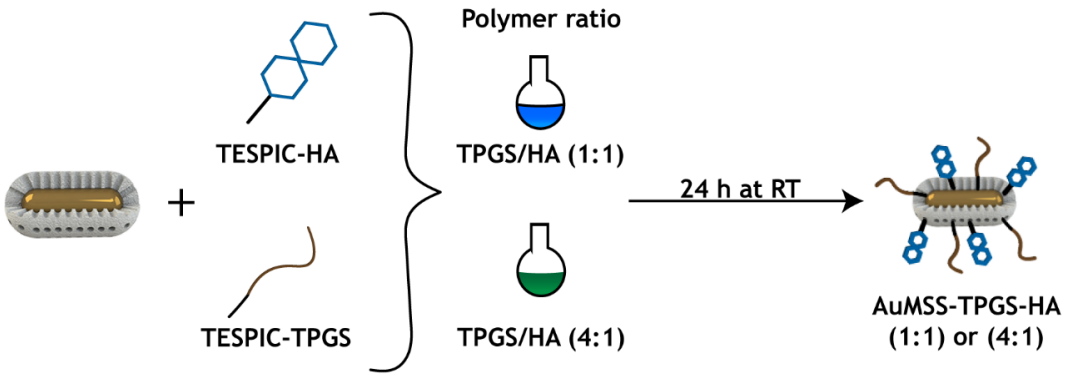

Figure 6 - Representation of the nanoparticles' functionalization with different ratios of TPGS and HA (1:1 and 4:1), RT - room temperature.

2.2.5. Characterization of nanocarriers' physicochemical properties

2.2.5.1. Morphological characterization and size analysis

The morphology of the coated and uncoated AuMSS nanorods was characterized by Transmission Electron Microscopy (TEM – Hitachi-HT7700, Japan). The nanoparticles samples were placed on formvar-coated copper grids and allowed to dry at room temperature. The images were acquired at an accelerating voltage of 80 kV. Afterward, nanoparticles total size, silica shell thickness, and gold core size were measured by using a specific software (Image J 2.0.0, NIH Image, USA).

2.2.5.2. Zeta potential analysis

The zeta potential measurements of both coated and uncoated AuMSS nanorods were performed by using a Zetasizer Nano ZS equipment (Malvern Instruments, Worcestershire, UK). All the measurements were performed in ultrapure water as well as in PBS at pH 7.4 and 5.6. The data was collected at 25 ºC in a disposable capillary cell.

2.2.5.3. Ultraviolet-visible spectroscopy analysis

The success of AuMSS nanorods synthesis was evaluated through the acquisition of the particles' UV-vis spectra, using an UV-vis spectrophotometer (Thermo Scientific EvolutionTM 201 Bio UV-vis Spectrophotometer, Thermo Fisher Scientific Inc., USA) at a 300 $nm.min^{-1}$ scanning rate, with a wavelength range from 190 to 1100 nm.

2.2.5.4. Fourier transform infrared spectroscopy analysis

Fourier transform infrared (FTIR) spectroscopy was used to evaluate the successful purification and functionalization of the AuMSS nanorods. For that purpose, FTIR spectra of the nanoparticles were acquired on a Nicolet iS10 spectrometer, with a 4 cm^{-1} spectral resolution from 400 to 600 cm^{-1} (Thermo Scientific Inc., Massachusetts, USA). Moreover, in all the acquired data a baseline correction and atmospheric suppression were performed to avoid any possible interferences. Data analysis was executed in the OMNIC spectra software (Thermo Scientific).

2.2.5.5. Thermogravimetric analysis

The polymer content on the AuMSS formulations was measured by performing the thermogravimetric analysis (TGA) of the samples. Briefly, uncoated or coated AuMSS nanorods were heated up to 600 ºC, at a heating rate of 10 ºC/min under an inert atmosphere on an SDT Q600 equipment (TA Instruments, USA), and the particles' weight losses were recorded along time.

2.2.6. *In vitro* photothermal measurements

The evaluation of the *in vitro* photothermal capacity of different AuMSS nanorods formulations was performed as previously reported in the literature (105). Briefly, the AuMSS nanoformulations at a concentration of 200 µg/mL or a control group without nanoparticles were irradiated with a NIR laser (808 nm, 1.7 W/cm^2). Then, the media' temperature variation was monitored at different times points (from 1 up to 10 min) by using a thermocouple sensor with an accuracy of 0.1 ºC.

2.2.7. Cytocompatibility assays

2.2.7.1. Cell viability

The HeLa or FibH cells' viability when incubated with coated and non-coated AuMSS nanorods was assessed through the resazurin-based assay (134). For that purpose, both cells lines were seeded into 96-well flat bottom culture plates at a density of 10 000 cells per well, with 200 µL of medium (DMEM-HG for Hela cells and DMEM-F12 medium for FibH cells), and left at 37 ºC with humid atmosphere containing 5% CO_2 for 24 h. Afterward, the cells were incubated with different concentrations (from 25 to 200 µg/mL) of AuMSS nanorods, AuMSS-TPHS-HA (1:1), and AuMSS-TPGS-HA (4:1). After 24, 48 and 72 h of incubation, the medium in each well was replaced with 110 µL of 10% (v/v) resazurin solution. After 4 h of incubation, the fluorescence of the produced resorufin was quantified with a spectrofluorometer (Spectramax Gemini XS, Molecular Devices LLC, USA) at an excitation/emission wavelength of λex=560 nm and λem=590

nm. Cells incubated with ethanol (99,9 %) were used as a positive control (K^+), whereas cells without nanoparticles' incubation were used as a negative control (K^-).

2.2.7.2. Hemolysis

Hemolysis experiments were performed according to previous reports in the literature to evaluate the nanoformulations' impact on the RBCs (137). EDTA stabilized blood samples were freshly obtained from adult mice. At first, the whole blood samples were centrifuged for 5 min at 500g and 4 °C and washed three times with NaCl solution (150 mM) to recover the RBCs. Subsequently, the RBCs were diluted in PBS, distributed by the test tubes and centrifuged. Next, 1 mL of AuMSS, AuMSS-TPGS-HA (1:1) or AuMSS-TPGS-HA (4:1) at different concentrations (100 and 200 µg/mL) were added to the RBCs suspension, and the samples were incubated at room temperature for 2 and 4 h. At the same time, a positive (K^+) and negative (K^-) control samples were prepared by adding 1 mL of Triton-X 100 and PBS to the RBCs suspension, respectively. All the samples were slightly shaken every 30 min to resuspend the RBCs and particles. After the incubation period, the samples were centrifuged for 5 min at 500g and 4 °C and the supernatants absorbance was measured at 570 nm to quantify the free hemoglobin. The RBCs hemolysis percentage was calculated using the following equation:

$$\text{Hemolysis (\%)} = \frac{\text{Sample Abs-Negative Control Abs}}{\text{Positive Control Abs-Negative Control Abs}}$$

2.2.7.3. HeLa cells live/dead assay

The cytocompatibility of the AuMSS, AuMSS-TPGS-HA (1:1), and AuMSS-TPGS-HA (4:1) nanorods was also evaluated by fluorescence microscopy through the Live/Dead assay (Invitrogen, Life Technologies, USA). This assay uses calcein acetozxmethyl (calcein AM) and propidium iodide dyes to allow the visualization of live and dead cells, respectively. Briefly, HeLa cells were seeded on µ-Slide 8 well Ibidi imaging plates (Ibidi GmbH, Germany), and incubated at 37 °C, in 5% CO_2 humidified atmosphere for 24 h. After that period, uncoated or coated AuMSS nanorods at concentration of 200 µg/mL were incubated with the HeLa cells, whereas cells non-exposed to nanoparticles were used as negative control (Control). After 48 h, cells were incubated with the staining solution according to the manufacturer's instructions, for 15–20 min, and analyzed on a confocal microscope (Zeiss LSM 710, Carl Zeiss, Germany).

2.2.8. Cellular uptake by HeLa and FibH cells

The uptake of AuMSS, AuMSS-TPGS-HA (1:1), and AuMSS-TPGS-HA (4:1) nanorods by HeLa or FibH cells was characterized by fluorescence spectroscopy, by adapting a method previously described in the literature (138). Initially, HeLa or FibH cells were seeded at a density of 8,000

cells per well in 96-well flat bottom culture plates. For 24 h, cells were cultured at 37 °C in a humid atmosphere containing 5% CO_2. Then FITC stained uncoated or coated AuMSS nanorods at 200 μg/mL were incubated for 2 and 4 h. Afterwards, cells were washed with ice-cold Krebs Ringer Buffer to remove the non-internalized particles and lysed with 1% Triton X-100 (30 min at 37 °C). The FITC fluorescence was quantified with a spectrofluorometer (Spectramax Gemini XS, Molecular Devices LLC, USA) at an excitation/ emission wavelength of λex=480 nm and λem=570 nm. Cells incubated only with Krebs Ringer Buffer were used as a negative control.

To further confirm the results, confocal laser scanning microscopy (CLSM) was performed to assess the nanoparticles internalization by HeLa cells, following a protocol previously described by Gaspar and co-workers (139). Consequently, 10 000 HeLa cells were seeded on μ-Slide 8 well Ibidi imaging plates (Ibidi GmbH, Germany), and incubated at 37 °C in 5% CO_2 humidified atmosphere. After 24 h, FTIC stained uncoated or coated AuMSS nanorods were incubated with the cells at a concentration of 200 μg/mL, for 4 h. Afterwards, cells were washed with PBS, fixed with PFA 4% (w/v) for 15 min, and washed again with PBS. Finally, cells were treated with WGA-Alexa Fluor® 594 and Hoechst 33342®, for cell cytoplasm and nucleus staining, respectively. Imaging experiments were performed in multi-track mode on a confocal microscope (Zeiss LSM 710, Carl Zeiss, Germany), where consecutive z-stacks were acquired. 3D reconstructions and image analysis were performed in Zeiss Zen 2010 software.

2.2.9. Characterization of the 2D cytotoxic profile of the nanoparticles

The AuMSSs cytotoxic effect was evaluated by the resazurin assay (103). To evaluate the NIR-induced cytotoxic activity of the AuMSS, AuMSS-TPGS-HA (1:1), and AuMSS-TPGS-HA (4:1) nanoformulations, were incubated with HeLa cells at 200 μg/mL, in the presence or absence of NIR laser irradiation. Briefly, the cells were seeded into a 96-well flat bottom culture plates at a density of 10 000 cells per well. After 24 h of incubation, coated and non-coated AuMSS nanorods were incubated with HeLa cells. After 6 h, the cells were irradiated with laser (808 nm, 1.7 W/cm^2) for 5 min. At 24 h of incubation, the cells' viability was evaluated by using the resazurin assay.

2.2.10. Statistical analysis

Data are presented as the mean ± standard deviation (s.d.). One-way analysis of variance (ANOVA) with the Student–Newman–Keuls post-test was used for multiple groups comparison. A p-value lower than 0.05 ($p<0.05$) was considered statistically significant. Statistical analysis was performed using GraphPad Prism v.6.0 software (Trial version, GraphPad Software, USA).

Chapter III

Results and Discussion

3. Results and Discussion

3.1. Synthesis and characterization of TESPIC-TPGS and TESPIC-HA polymers

The HA is a hydrophilic and linear polysaccharide that consists on repeated N-acetylglucosamine and glucuronic di-saccharide units (140). Additionally, HA is biocompatible, biodegradable, and non-immunogenic. Moreover, HA can act as a targeting moiety due to its strong affinity to the CD44-recetors, which are overexpressed on the membrane of cancer cells (141). Further, despite these receptors can also be found at lower levels in healthy cells, they are in a quiescent state that do not interact with HA (142). On the other side, TPGS is a water-soluble vitamin E derivative that has an amphiphilic nature and can act as solubilizer. Further, the TPGS can also inhibit the P-gp, a drug efflux pump overexpressed in cancer cells, and therefore improve the therapeutics action (143). Herein, it was hypothesized that the AuMSS nanorods functionalization with HA and TPGS may have the potential for overcoming the AuMSS nanorods' limited colloidal stability, improve their half-life time in blood circulation, enhance their selectivity towards HeLa cancer cells, and consequently potentiate the nanoparticles therapeutic effect.

For that purpose, TPGS and HA were chemically modified to allow the posterior grafting on the AuMSS nanorods' surface. The modification of both polymers was achieved by promoting the TESPIC linkage to the polymer backbone through a hydrogen-transfer nucleophilic addition reaction (Figure 7) (144).

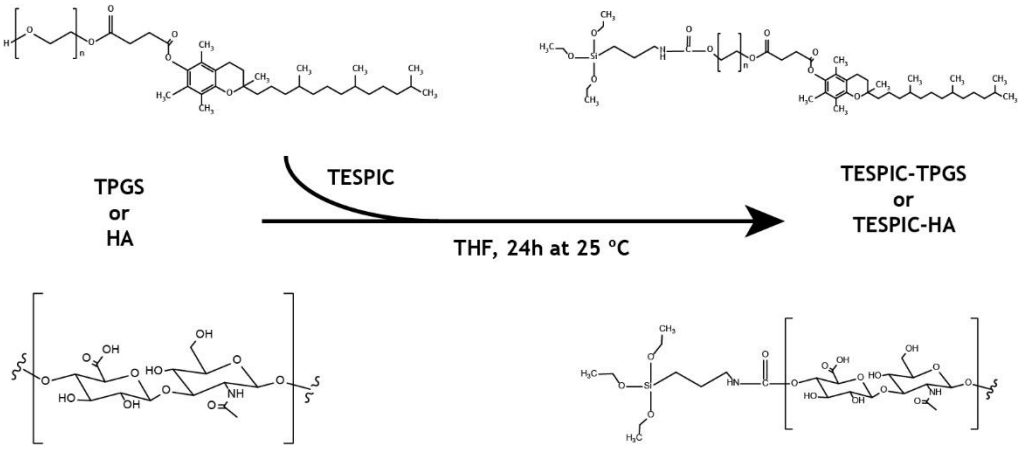

Figure 7 - Synthesis schematic of TESPIC-TPGS and TESPIC-HA polymers.

The successful synthesis of the silane-modified TPGS and HA polymers was confirmed through FTIR and NMR analysis (Figure 8). The FTIR spectrum of TPGS shows the characteristic peaks at 1740 cm^{-1} and 1105 cm^{-1} corresponding to the vibration peak of C=O bond and C–O stretching vibration, respectively (145). After the modification with TESPIC, the spectrum showed a distinctive absorption peak in the 1680-1640 cm^{-1} region, which is coherent with the newly formed secondary amides.

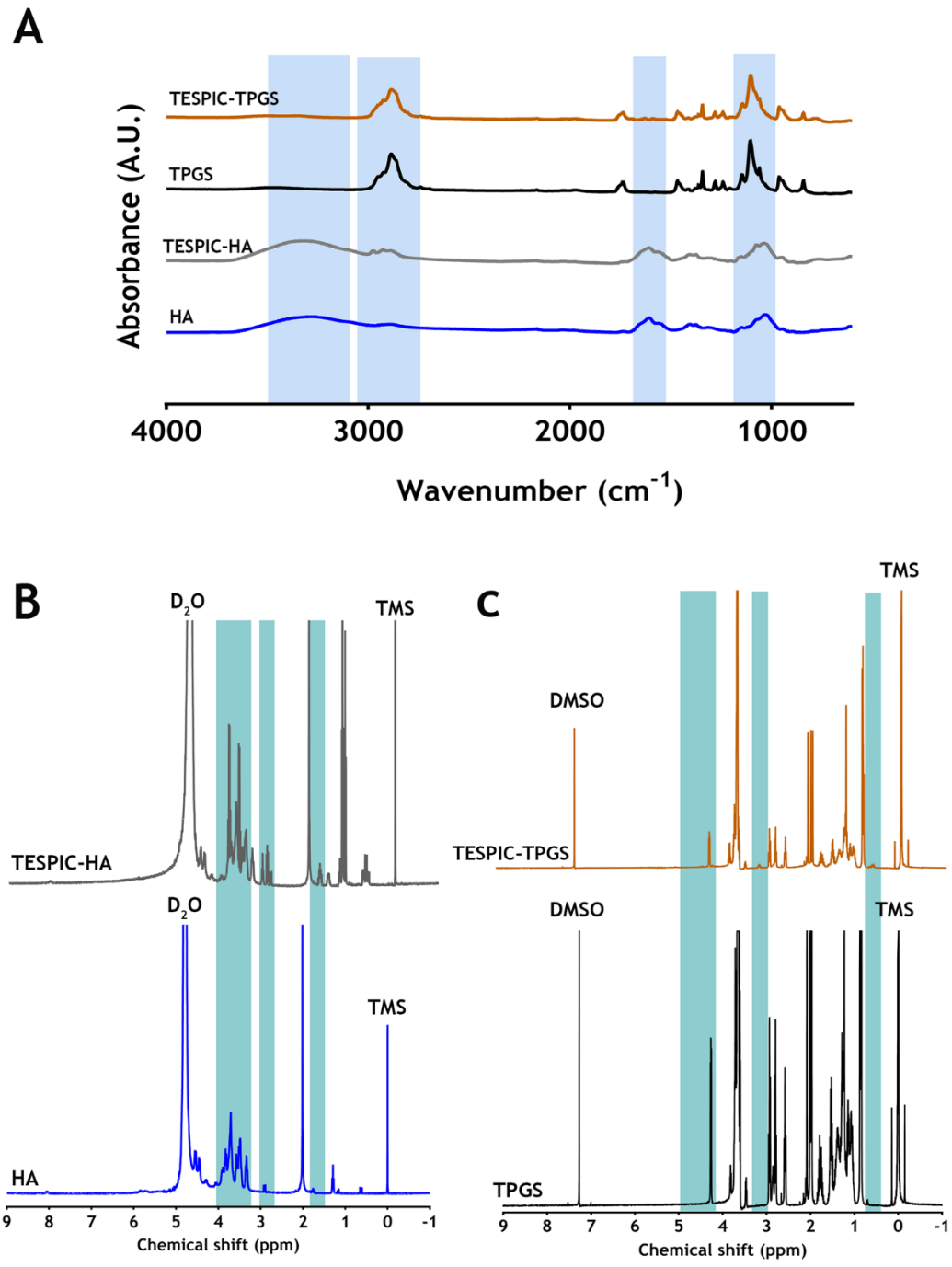

Figure 8 - FTIR (A) and NMR (B and C) spectra of TPGS, TESPIC-TPGS, HA and TESPIC-HA polymers.

Additionally, the introduction of the silane moiety on the TPGS backbone also altered the spectrum in the 1110-1050 cm^{-1} region due to the absorption band of the Si-O-C bonds. On the other hand, the HA spectrum exhibits a broad O–H stretching bond at 3200–3650 cm^{-1}, a shoulder peak around 2900 cm^{-1} associated with CH_2 vibration, C=O stretching bond at 1100–1300 cm^{-1}, and a CO-NH (amide) bond at 1630–1680 cm^{-1} (146). After reacting with TESPIC, the peak at 1100-1300 cm^{-1} region was enhanced owing to the absorption band of the Si-O-C bonds (Figure 8 A). These results were further confirmed by the NMR analysis (Figure 8 B and C).

The NMR spectrum of TPGS shows the proton peaks characteristic of the PEG chain methylene groups (CH_2) at 3.65 ppm. After the TPGS modification, it was possible to observe the addiction of the TESPIC characteristic methylene groups (Si-CH_2, 0.81 ppm; CH_2-NH, 3.18 ppm) (Figure 8B). On the other side, the HA data show the characteristic proton peaks at approximately 2 ppm (N-acetyl group), 3.2-4.2 (sugar rings H), and 4.35–4.71 (anomeric H)(147). After the modification, besides the peaks related to HA it was also possible to observe the TESPIC related peaks (Si-CH_2, 0.81 ppm; CH_2-NH, 3.18 ppm) (Figure 8 C).

3.2. Synthesis and characterization of AuMSS nanorods

The AuMSS nanorods were synthesized by using a seed-mediated methodology (42, 58, 133). The synthesis procedure is divided in three main steps: firstly, occurs the production of small spherical gold particles (seeds), then this solution is added to a growth solution to trigger the formation of gold nanorods, and finally is performed the mesoporous silica shell coating, using CTAB as a soft template to promote the pores formation. The successful synthesis of AuMSS nanorods was confirmed through TEM (Figure 9). The analysis of the TEM images demonstrate that the gold-core present a mean length and width of 50 ± 7 nm and 16 ± 3 nm, respectively. Such corresponds to an aspect ratio (AR) of 3.1, which is within the AR ranges (3-4) often described has ideal for PTT applications (148). Additionally, the AuMSS nanorods present a mean mesoporous silica shell thickness of ~36 nm resulting in particles with a total length and width of 85 ± 12 and 64 ± 8 nm, respectively (Figure 9 A1 and A2). Besides that, the functionalization with different ratios of TPGS and HA (1:1 and 4:1) nanorods does not shows any significant variations on the particle overall size (Figure 9 B1, B2, C1 and C2) (123). Nevertheless, the overall size of the AuMSS formulations is compatible with the intravenous administration, allowing them to exploit the EPR and therefore to accumulate passively in the tumor tissue. The successful formation of the mesoporous silica coating and removal of the cytotoxic CTAB molecules was confirmed by FTIR (Figure 10). The AuMSS FTIR spectrum shows the mesoporous silica shell characteristic peaks in the 1100 to 750 cm^{-1} region, which corresponds to Si-O-Si, Si-O and Si-OH vibrations (134).

Additionally, after the purification procedure, the two characteristic peaks of CTAB, the C-H vibration between 2950 cm^{-1} and 2850 cm^{-1} and CH_3-N^+ deformation at 1450-1500 cm^{-1}, disappear (42). Consequently, this data indicates the successful removal of the CTAB molecules from the AuMSS nanorods, which improves the nanosystem biosafety and biocompatibility.

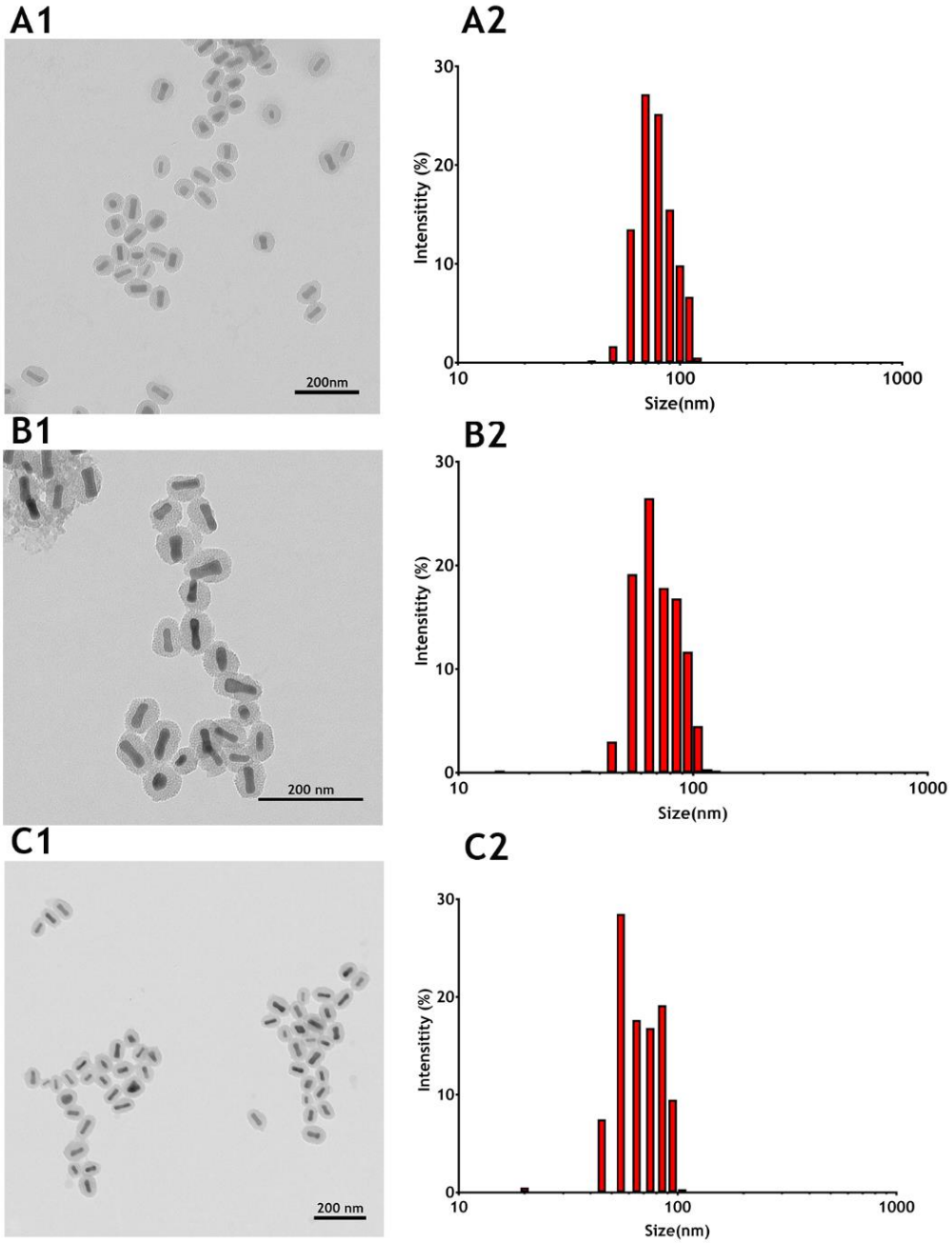

Figure 9 - AuMSS nanoformulations morphology and size distribution. TEM images of AuMSS (A1), AuMSS-TPGS-HA (1:1) (A2) and AuMSS-TPGS-HA (4:1) (C1) nanorods. Size distribution (length and width included, with n=300) of AuMSS (A2), AuMSS-TPGS-HA (1:1) (B2) and AuMSS-TPGS-HA (4:1) (C2) nanoformulations.

3.3. Functionalization of the AuMSS nanorods

The AuMSS nanorods were functionalized by promoting the chemical grafting of the TESPIC-TPGS and TESPIC-HA silane derivatives on the surface of the AuMSS nanorods. During this process, the TESPIC modified polymers condensate with the silanol (Si-OH) groups available on the surface of the AuMSS nanorods. The nanoparticles' surface functionalization was confirmed by recording the changes on the zeta potential (Figure 11 A). The AuMSS nanorods displayed a negative surface charge, -28 ± 10 mV, attributed to the presence of negatively charged silanol groups on the mesoporous silica surface. On the other hand, the AuMSS-TPGS-HA (1:1) and AuMSS-TPGS-HA (4:1) nanoformulations presented a surface charge of -3 ± 5 mV and 11 ± 2 mV, respectively. The surface charge measurements were also performed in PBS at pH 7.4 and 5.6, the obtained results demonstrate that the functionalized nanoparticles remain with a surface charge within the neutral range (± 10 mV) (137, 149). As described in the literature, the nanomaterials' surface charge plays an important role on their biological performance, since it highly influences the nanoparticles' blood circulation, biocompatibility and pharmacokinetic profile. Moreover, nanoparticles with a neutral charge (± 10 mV) are considered ideal for biological applications since they exhibit a lower interaction with the reticuloendothelial system (RES) and the longest blood circulation time (150). Additionally, the successful linkage of the polymers to the nanoparticles surface was also evaluated by FTIR analysis (Figure 10). The FTIR spectra of both formulations present the three characteristic peaks of the mesoporous silica shell in the 1100 to 750 cm^{-1} region. Additionally, after the polymers grafting it is also possible to observe the TPGS and HA peaks in around the 2900 cm^{-1} and 1630–1680 cm^{-1}, respectively.

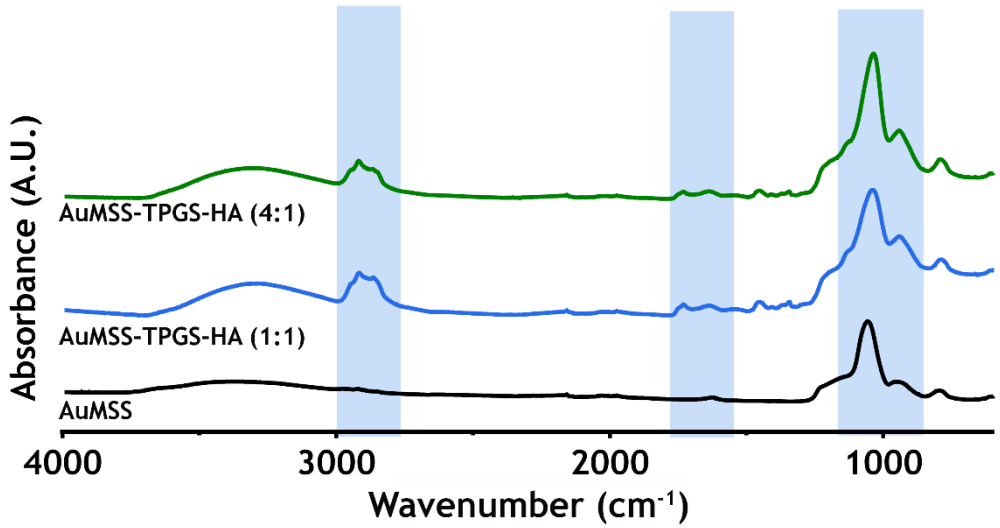

Figure 10 - FTIR spectra of AuMSS, AuMSS-TPGS-HA (1:1) and AuMSS-TPGS-HA (4:1).

The successful attachment of the polymeric chains to the AuMSS nanorods' surface and the determination of the polymer content in each of the AuMSS formulations was confirmed by performing a thermogravimetric analysis (Figure 11 B). The recorded weight losses for AuMSS nanorods were approximately 5% and can be attributed to the loss of the hydroxyl groups (-OH) on the surface of the particles or to the evaporation of water adsorbed in the interior mesopores pores. On the other side, the functionalized AuMSS nanorods presented a weight loss of 26% and 22% for the 1:1 and 4:1 formulations, respectively. These weight losses are attributed to the polymer pyrolysis, corroborating the successful introduction of TPGS and HA on the surface of the AuMSS nanorods.

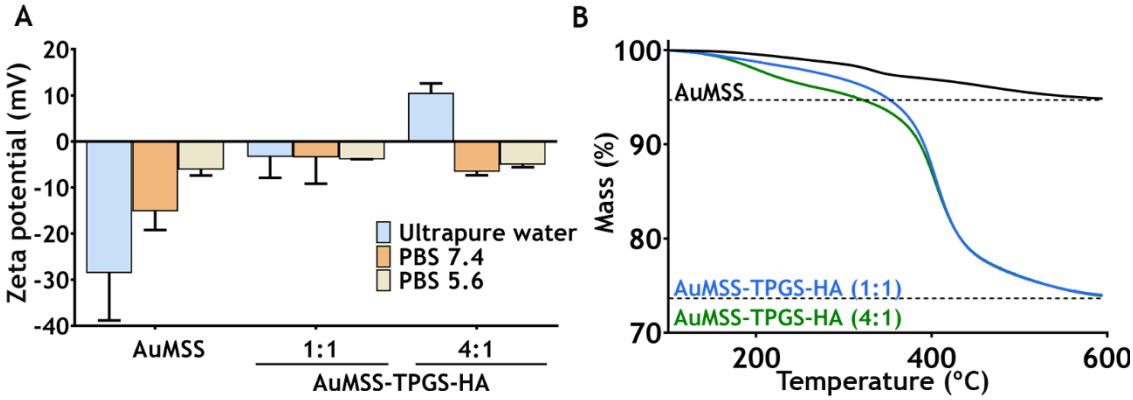

Figure 11- Physicochemical characterization of AuMSS formulations. (A) Surface charge analysis of AuMSS, AuMSS-TPGS-HA (1:1), and AuMSS-TPGS-HA (4:1) nanoformulations in different media, such as ultrapure water and PBS at pH 7.4 and 5.6, n=3. (B) TGA analysis of AuMSS, AuMSS-TPGS-HA (1:1), and AuMSS-TPGS-HA (4:1) nanoformulations.

3.4. *In vitro* evaluation of the AuMSS nanorods' photothermal capacity

The AuMSS nanorods potential to mediate a PTT effect was initially assessed by acquiring its UV-vis absorption spectrum (Figure 12 A). The AuMSS nanorods presented two absorption peaks at 520 nm and 780 nm (*i.e.* NIR region). The two observed absorption bands are characteristic from the transverse and longitudinal plasmon resonances of gold nanorods. In fact, the absorption band at 780 nm is coherent with the obtained gold nanorods' AR (3.1) and it is compatible with PTT applications (absorption in the NIR region). Furthermore, the nanoparticles' functionalization with TPGS and HA polymers did not induce significant alterations in their absorption peaks. Then, the photothermal capacity of the AuMSS formulation was investigated by measuring the temperature changes induced by the nanoparticles upon NIR laser irradiation (Figure 12 B). For that purpose, the formulations were exposed to a NIR light (808 nm, 1.7 W/cm^2) for 1 to 10 min, and the temperature variations were recorded. In the Figure 12 B, it is possible to observe, that the AuMSS, AuMSS-TPGS-HA (1:1), and AuMSS-TPGS-HA (4:1) nanorods can mediate an increase in the temperature when irradiated with the NIR laser for up to 10 min. Further, the AuMSS functionalization did not

affect the PTT capacity of the gold nanorods, since all the nanoformulations were capable to produce a temperature variation superior to 20 ºC at the end of the experiment. Such findings indicate that the AuMSS nanorods have a good colloidal stability since the nanoparticles' aggregation is often linked to changes on the absorption spectra and consequently alterations on their PTT capacity. More importantly, the recorded temperature variations indicate that the AuMSS nanorods upon NIR light irradiation can cause the cell death by inducing the disruption of the cell membrane and alterations on the metabolic pathways (115).

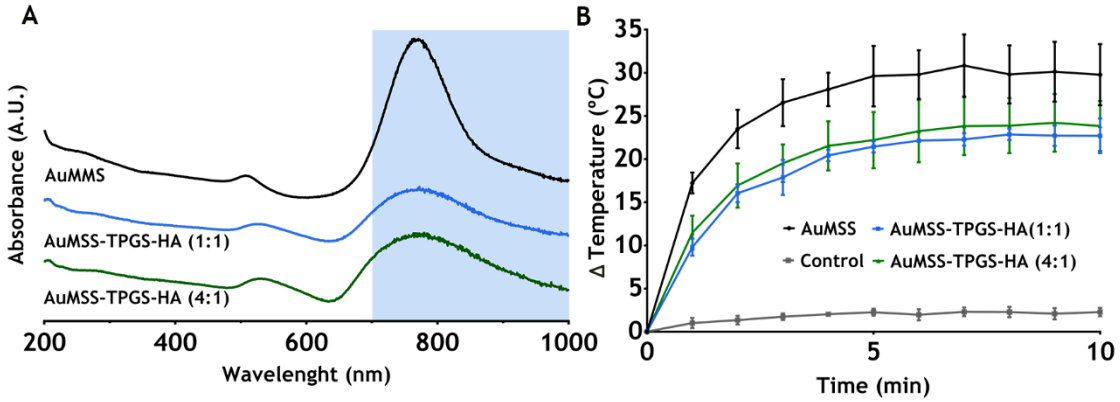

Figure 12 - Characterization of the AuMSS nanoformulations' *in vitro* PTT capacity. (A) UV-vis spectra of AuMSS nanorods and its derivatives. (B) Temperature variation curves of AuMSS and AuMSS derivatives in ultrapure water under NIR laser (808 nm, 1.7 W/cm^2) irradiation for 10 min. Control: ultrapure water. Data are presented as mean ± s.d..

3.5. Nanoparticles biocompatibility

3.5.1. Cell viability

The biocompatibility of AuMSS nanorods and its formulations was evaluated both on HeLa cells and FibH cells (Figure 13). For that purpose, the different nanoparticle formulations were incubated for 24, 48 and 72 h, at concentrations ranging from 25 up to 200 µg/mL, and the cellular viability was measured using the resazurin assay. According to the ISO 10993-5 "*Biological evaluation of medical devices - Part 5: Tests for in vitro cytotoxicity*", a material has a cytotoxic effect when the cell viability is reduced by more than 30%. So, as can be observed in Figure 13, the results show that the AuMSS nanorods are biocompatible at concentrations up to 200 µg/mL for both cell lines. These results are in concordance with other reports available in the literature for AuMSS based nanomedicines as well as with the TPGS and HA safety profile (Food and Drug Administration (FDA)-approved polymers for biomedical applications) (42, 95, 109, 151).

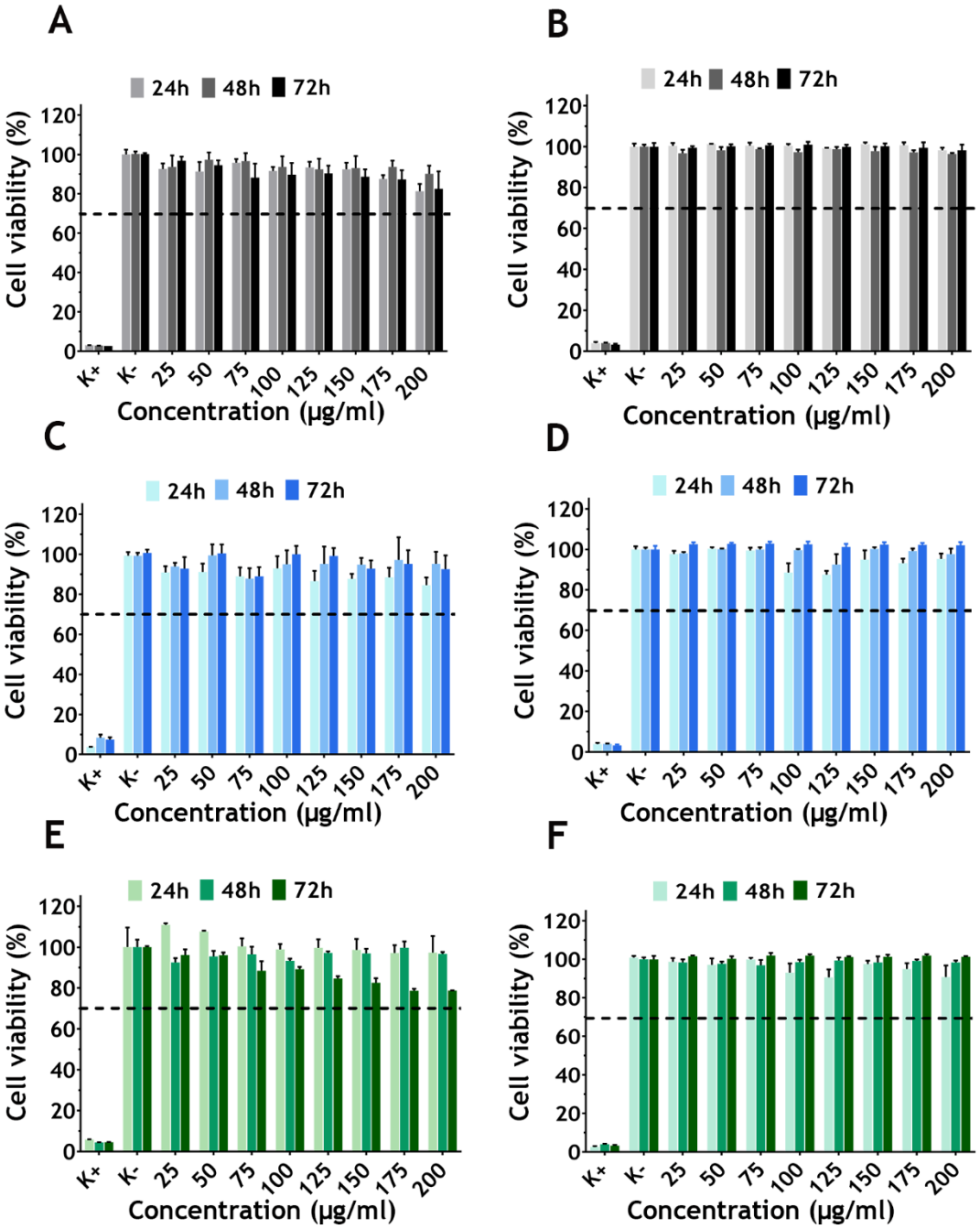

Figure 13 - Evaluation of AuMSS nanoformulations' cytocompatibility at 24, 48 and 72 h on FibH (A, C and E) and HeLa cells (B, D and F). Cytocompatibility analysis for AuMSS nanorods (A) and (B), AuMSS-TPGS-HA (1:1) (C) and (D), AuMSS-TPGS-HA (4:1) (E) and (F). Positive control (K+): cells treated with EtOH; negative control (K-): cells without nanoparticles incubation. Data are presented as mean ± s.d..

3.5.2. HeLa cells live/dead assay

Further, Live/Dead assays were performed to confirm the AuMSS nanoformulations cytocompatibility with HeLa cells (Figure 14). The attained CLSM images demonstrated that cells remain viable (green channel) when seeded with the nanoparticles, with only few dead cells (red channel) being observed in each condition, including the control. These observations corroborate the data obtained in the resazurin assay, thus supporting the cytocompatibility of these nanoparticles.

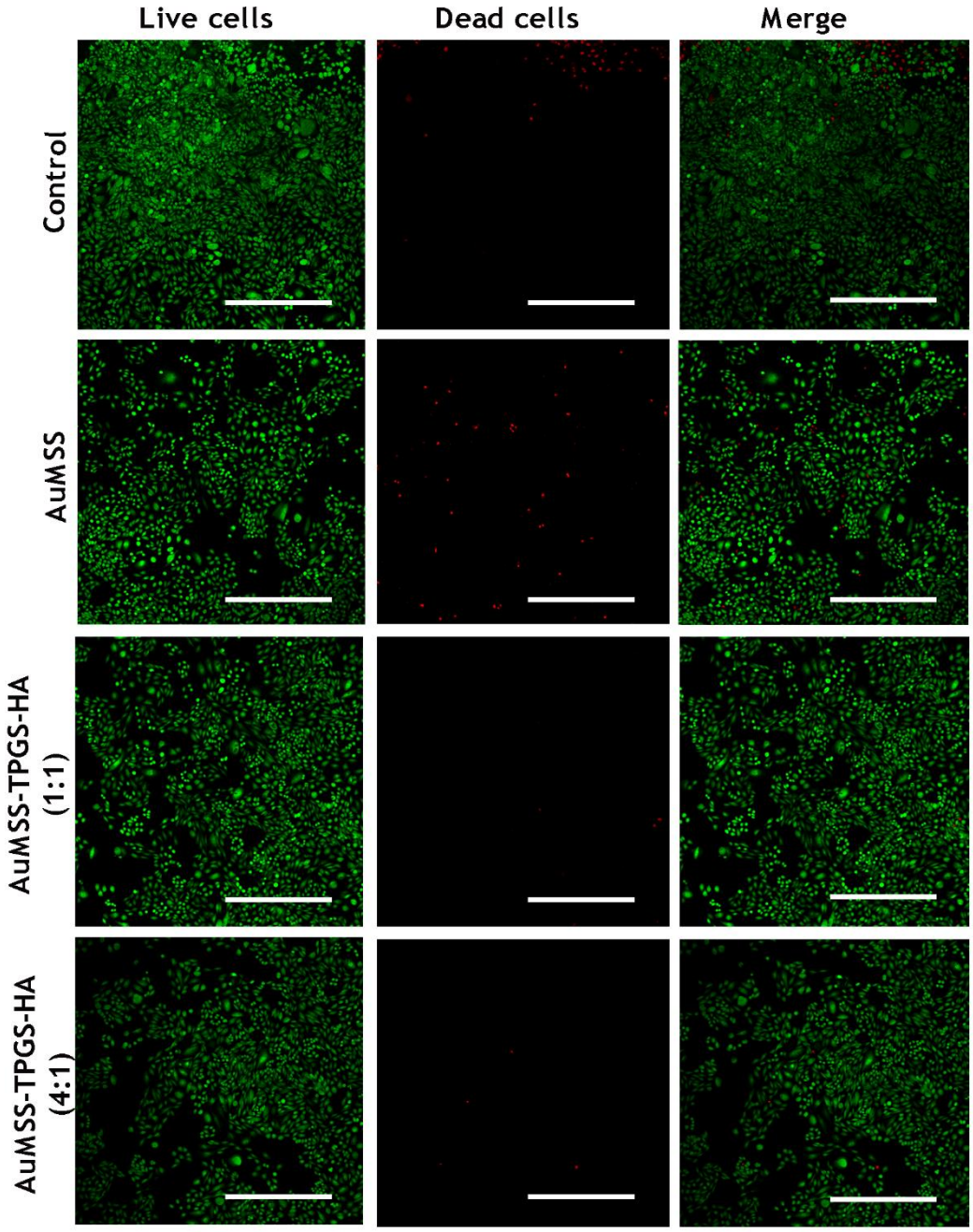

Figure 14 - Live/Death CLSM images of HeLa cells incubated with the different AuMSS nanorods formulations. Control: Cells incubated with medium. Green channel: Calcein stained cells; Red channel: Propidium Iodide stained cells. Scale bar: 500 µm.

3.5.3. Hemolysis

Another important parameter in the nanoparticles' biosafety is their hemocompatibility (Figure 15). Therefore, the RBCs lysis was quantified upon incubation with the different AuMSS formulations (100 and 200 µg/mL) for 2 and 5h. According to the ISO/TR 7406 a biomaterial is considered non-toxic and biologically safe if the hemolysis percentage is inferior to 5% (152). Therefore, the obtained results demonstrate that the non-coated AuMSS nanorods at 200 µg/ml are hemolytic since more than 5% of hemoglobin was released after 2 and 5 h of incubation. On the other side, both functionalized formulations, AuMSS-TPGS-HA (1:1) and AuMSS-TPGS-HA (4:1) shown to be non-hemolytic, being registered less than 1% and 2.5% of hemolysis after 2 and 5 h of incubation, respectively, even when at the concentration of 200 µg/mL. Nevertheless, after 5 h of incubation, the AuMSS-TPGS-HA (4:1) formulation appears to have an improved hemocompatibility in both tested concentrations, when compared to the AuMSS-TPGS-HA (1:1) formulation. This result can be explained by the higher amount of TPGS in this formulation and by its antioxidant properties, which will protect the RBCs cell membrane and consequently decrease the hemolysis (153).

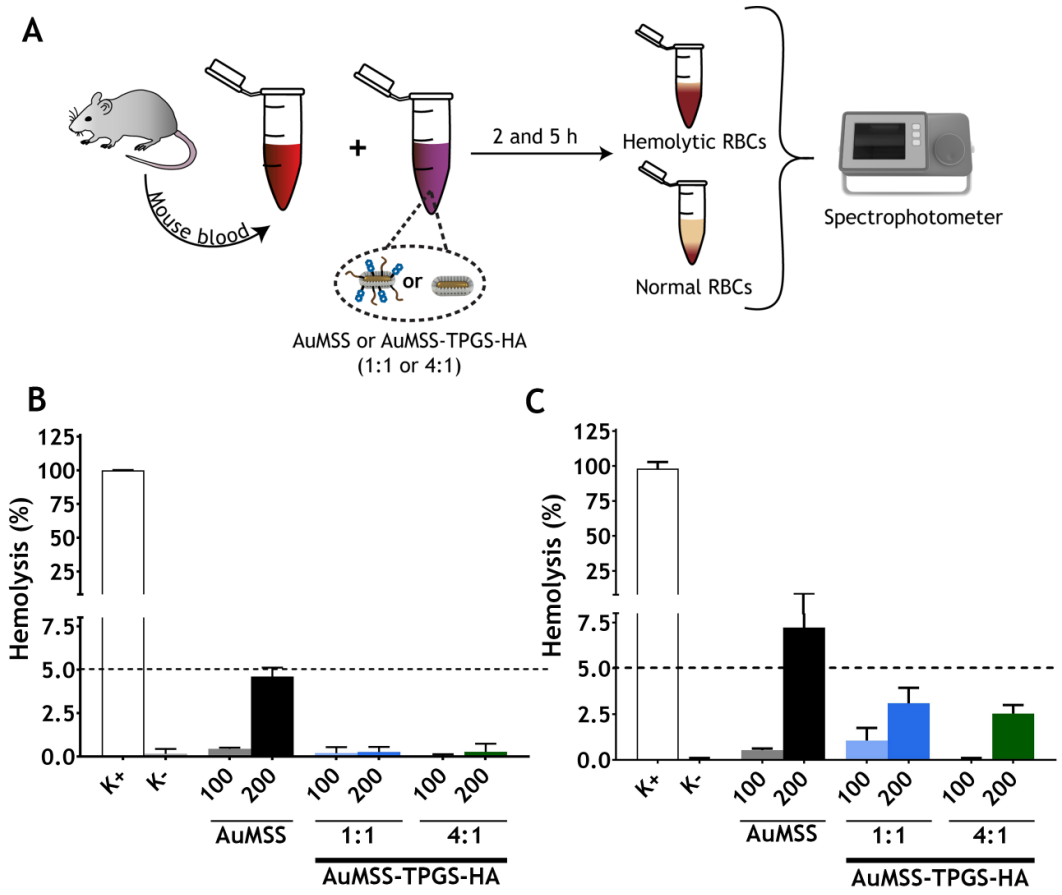

Figure 15 - Analysis of the AuMSS nanorods' hemocompatibility. (A) Schematics of the hemocompatibility assays. Analysis of the RBCs lysis upon incubation with different concentrations of AuMSS nanoformulations at 2 h (B) and 5 h (C), respectively. Data are presented as mean ± s.d..

3.5.4. Cellular uptake by HeLa and FibH cells

After evaluating the cytocompatibility of the AuMSS nanorods formulations, their cellular uptake by HeLa cancer cells was evaluated by CLSM and fluorescence spectroscopy. The nanoparticles uptake by cancer cells is one of the most challenging barriers that nanomedicines must overcome. Therefore, prior to this assay, non-coated and coated AuMSS nanorods were stained with FITC to allow the nanoparticles tracking. Then, the different AuMSS nanorods formulations were incubated for 4 h with HeLa cells and confocal images were acquired. The CLSM images show that the nanoparticles can be efficiently uptaken by HeLa cancer cells, being observed the FITC fluorescence on the cells' cytoplasm (Figure 16).

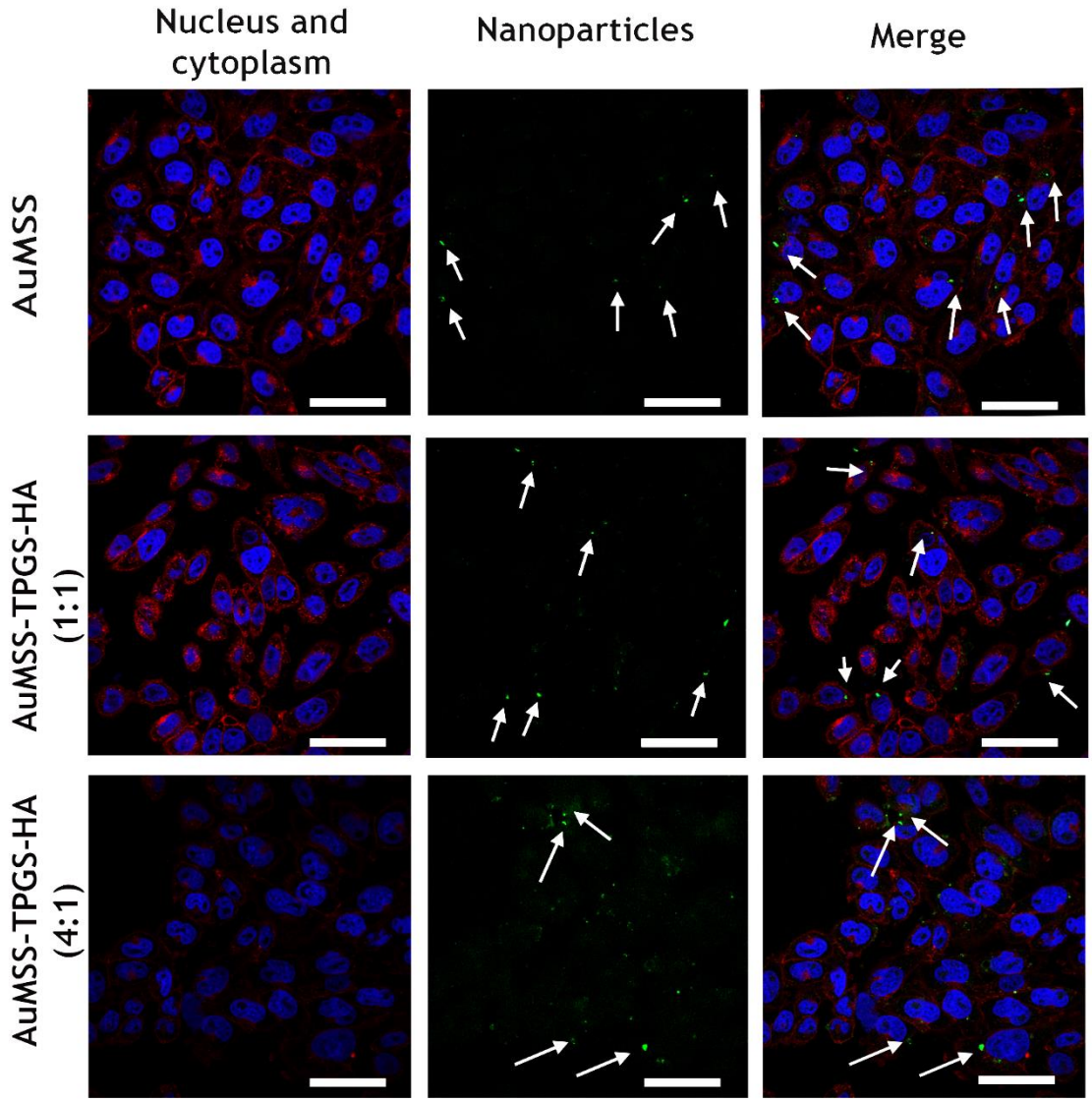

Figure 16 - Representative confocal microscopy images of the AuMSS formulations uptake by HeLa cells. The white arrows are pointing to the internalized nanoparticles. The scale bar corresponds to 50 μm. Blue channel: Hoechst 33342® stained cell nucleus; red channel: WGA-Alexa Fluor 594® stained cell cytoplasm; green channel: FITC labeled nanoparticles.

Additionally, the HA targeting capacity was also evaluated by measuring the fluorescence of the FITC labelled AuMSS nanoformulations in HeLa (CD44 overexpressing cell line) and FibH (low CD44 expression) cells through fluorescence spectroscopy (Figure 17). As it can be observed in the Figure 16 B, after 4 h of incubation with the nanoparticles, the HeLa cells incubated with FITC stained AuMSS-TPGS-HA (1:1) and (4:1) nanorods presented a higher fluorescence intensity than that of the FibH cells. This result may be explained by the AuMSS surface modification, particularly the grafting of HA, since it acts as a targeting moiety to the CD44 receptors which are highly expressed in HeLa cells. Further, it is worth to notice that the AuMSS-TPGS-HA (4:1) was the formulation that presented the lowest internalization on FibH cells, without being observed any significant impact on its uptake by the HeLa cancer cells. Therefore, this formulation can render a superior therapeutic performance with minimal accumulation on healthy cells. Such preferential internalization is in accordance with other reports available in the literature, where the nanoparticles functionalization with HA increased their cellular uptake by cancer cells overexpressing the CD44 (154, 155).

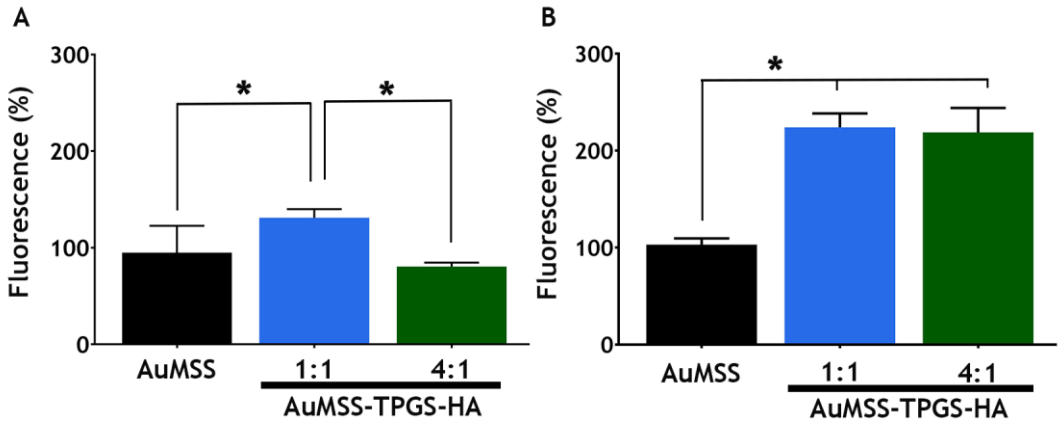

Figure 17 - Fluorescence spectroscopy analysis of uncoated and coated AuMSS nanorods uptake by FibH (A) and HeLa cells (B). The fluorescence was normalized towards the AuMSS nanorods group.

3.5.5. Characterization of the AuMSS nanorods phototherapeutic effect

For evaluating the PTT potential of the AuMSS formulations, the cytotoxic profile towards HeLa cells was assessed upon irradiation with NIR light (Figure 18). For that purpose, the cells were incubated with AuMSS formulations at a concentration of 200 µg/mL and irradiated with the NIR laser irradiation for 5 min. In Figure 18, it can be observed that the photothermal effect mediated by uncoated and coated AuMSS nanorods induced a decrease in the cancer cells viability to values inferior to 5%. Besides that, no significant differences were observed between the groups treated with the different AuMSS nanoformulations. Such is in accordance with the previously obtained data, where all the AuMSS formulations could mediate a temperature increase of more than 20 °C. In fact, it is described that hyperthermia treatments that reach

temperatures superior to 45 °C induce the cancer cells' death by causing irreversible cellular and DNA damage, protein denaturation, and disruption of the cellular membranes (156).

The HeLa cells death mediated by the AuMSS nanorods' photothermal effect was further confirmed by the CLSM images of the Live/Dead assays. The Live/Dead images clearly show a high number of dead cells after the AuMSS nanorods irradiation with the NIR laser. In this way, the obtained results confirm that the AuMSS-TPGS-HA formulations can produce an on-demand therapeutic effect upon NIR light irradiation.

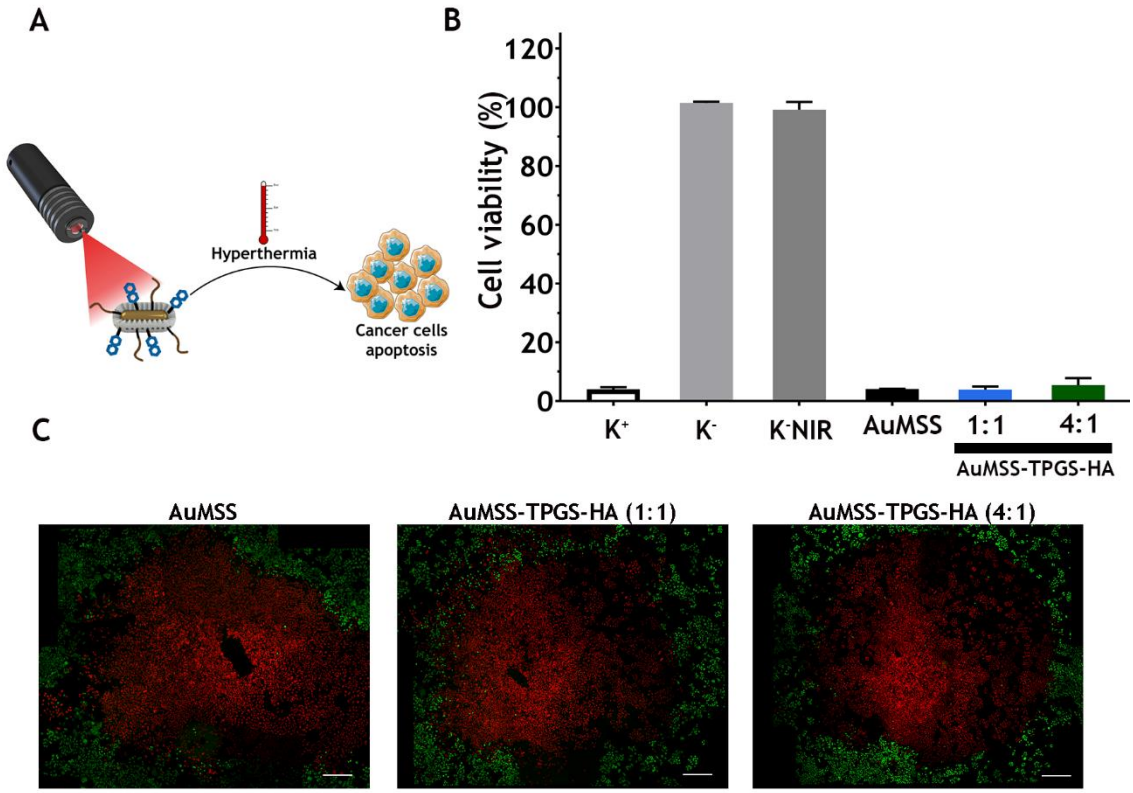

Figure 18 - Cytotoxic effect of AuMSS nanoformulations in HeLa cells. (A) Schematic representation of AuMSS nanoformulations cytotoxic activity upon NIR irradiation (808 nm, 1.7 W/cm^2, 5 min). (B) Cytotoxic activity of AuMSS, AuMSS-TPGS-HA (1:1) and AuMSS-TPGS-HA (4:1) at concentrations of 200 µg/mL. (K^+): cells treated with EtOH. (K^-): non-irradiated HeLa cells and (K^-+NIR): HeLa cells without particles incubation upon NIR irradiation (808 nm, 1.7 W/cm^2, 5 min). (C) Live/Death CLSM images of the cytotoxic activity of AuMSS nanoformulations at concentrations of 200 µg/mL Green channel: Calcein stained cells; Red channel: Propidium Iodide stained cells. Scale bar: 500 µm.

Chapter IV

Conclusions and Future Perspectives

4. Conclusion

Nowadays, despite all the efforts, cancer still remains as one of the main health problems affecting the population of the world. Therefore, a plethora of new therapeutic approaches aimed to improve cancer treatments have been under investigation. In this field, the application of NIR-absorbing nanomaterials for mediating the cancer PTT has been receiving a lot of interest due to their site-specific activation and on-demand therapeutic effect that can minimize the damages induced on the surrounding healthy tissues.

Among the different nanostructures capable of mediating the cancer PTT, AuMSS nanoparticles display advantageous physicochemical, biological, and optical properties that make them promising nanoplatforms for cancer therapy. The AuMSS nanorods are multifunctional nanomaterials that can act simultaneously as drug delivery, photothermal, and bioimaging agents. However, these nanomaterials display some limitations that hinder their direct application in cancer PTT, such as the limited blood circulation time, colloidal stabilityand selectivity to the cancer cells.

Taking this into consideration, in this dissertation, the TPGS and HA were combined for the first time to functionalize AuMSS nanorods with the objective to increase the nanoparticles biological performance and selectivity towards cancer cells. The obtained results demonstrate that the AuMSS nanorods functionalization did not impact on the nanorods overall size and on their PTT capacity. Further, the polymers grafting onto the nanoparticles improved their surface charge by inducing its neutralization (±10 mV). On the other hand, the *in vitro* cellular assays showed that all the AuMSS nanoformulations were biocompatible at concentrations up to 200 µg/mL. Moreover, the AuMSS-TPGS-HA (4:1) nanorods showed the lower hemolysis rate at both tested concentrations, when compared with AuMSS and AuMSS-TPGS-HA (1:1). Additionally, the HA functionalization (1:1 and 4:1 ratios) improved the nanoparticles internalization by CD44 overexpressing cervical cancer cells, particularly the AuMSS-TPGS-HA (4:1) nanorods that also presented the lower internalization by health FibH cells. Finally, both formulations have shown to be capable of mediating an on-demand photothermal effect that induced the HeLa cancer cells death. Overall, the attained data support the application of the AuMSS-TPGS-HA nanorods as targeted multifunctional theragnostic nanomedicines.

In the near future the AuMSS-TPGS-HA nanorods' capacity to encapsulate and deliver anticancer drugs will be characterized to further increase the particles therapeutic potential. Moreover, the combination of PTT and chemotherapy will be characterized both with 2D and 3D cancer cell culture models. Then, the most promising formulation will proceed to *in vivo* assays to explore the biopolymers potential to improve the nanoparticles' biodistribution as well as to characterize the AuMSS biosafety and anti-tumoral effect.

Chapter V

References

5. References

1. Nagai H, Kim YH. Cancer prevention from the perspective of global cancer burden patterns. J Thorac Dis. 2017;9(3):448-51.

2. Bray F, Ferlay J, Soerjomataram I, Siegel RL, Torre LA, Jemal A. Global cancer statistics 2018: GLOBOCAN estimates of incidence and mortality worldwide for 36 cancers in 185 countries. CA Cancer J Clin. 2018;68(6):394-424.

3. Siegel RL, Miller KD, Jemal A. Cancer statistics, 2019. CA Cancer J Clin. 2019;69(1):7-34.

4. Miranda N GM, Andrade C, Santos G. Programa Nacional para as Doenças Oncológicas. Direção-Geral da Saúde. 2017.

5. Cancer Facts & Figures. American Cancer Society. 2019.

6. Pan M-H, Chiou Y-S, Wang Y-J, Ho C-T, Lin J-K. Multistage carcinogenesis process as molecular targets in cancer chemoprevention by epicatechin-3-gallate. Food Funct. 2011;2(2):101-10.

7. Zou W. Immunosuppressive networks in the tumour environment and their therapeutic relevance. Nat Rev Cancer. 2005;5(4):263-74.

8. Choi H, Moon A. Crosstalk between cancer cells and endothelial cells: implications for tumor progression and intervention. Arch Pharm Res. 2018;41(7):711-24.

9. Hanahan D, Weinberg RA. The hallmarks of cancer. Cell. 2000;100(1):57-70.

10. Hanahan D, Weinberg RA. Hallmarks of cancer: the next generation. Cell. 2011;144(5):646-74.

11. Gutschner T, Diederichs S. The hallmarks of cancer. RNA Biol. 2012;9(6):703-19.

12. Amin ARMR, Karpowicz PA, Carey TE, Arbiser J, Nahta R, Chen ZG, et al. Evasion of anti-growth signaling: A key step in tumorigenesis and potential target for treatment and prophylaxis by natural compounds. Semin Cancer Biol. 2015;35:S55-S77.

13. Fulda S. Tumor resistance to apoptosis. Int J Cancer. 2009;124(3):511-5.

14. Jafri MA, Ansari SA, Alqahtani MH, Shay JW. Roles of telomeres and telomerase in cancer, and advances in telomerase-targeted therapies. Genome Med. 2016;8(1):69.

15. Baudino TA. Targeted Cancer Therapy: The Next Generation of Cancer Treatment. Curr Drug Discov Technol. 2015;12(1):3-20.

16. DeSantis CE, Lin CC, Mariotto AB, Siegel RL, Stein KD, Kramer JL, et al. Cancer treatment and survivorship statistics, 2014. CA Cancer J Clin. 2014;64(4):252-71.

17. Moreira AF, Dias DR, Correia IJ. Stimuli-responsive mesoporous silica nanoparticles for cancer therapy: A review. Microporous Mesoporous Mater. 2016;236:141-57.

18. Nurgali K, Jagoe RT, Abalo R. Editorial: Adverse Effects of Cancer Chemotherapy: Anything New to Improve Tolerance and Reduce Sequelae? Front Pharmacol. 2018;9:245.

19. Gillet JP, Gottesman MM. Mechanisms of multidrug resistance in cancer. Methods Mol Biol. 2010;596:47-76.

20. Callaghan R, Luk F, Bebawy M. Inhibition of the multidrug resistance P-glycoprotein: time for a change of strategy? Drug Metab Dispos. 2014;42(4):623-31.

21. Misra R, Acharya S, Sahoo SK. Cancer nanotechnology: application of nanotechnology in cancer therapy. Drug Discov Today. 2010;15(19-20):842-50.

22. Kolovskaya OS, Zamay TN, Belyanina IV, Karlova E, Garanzha I, Aleksandrovsky AS, et al. Aptamer-Targeted Plasmonic Photothermal Therapy of Cancer. Mol Ther Nucleic Acids. 2017;9:12-21.

23. Liu Y, Bhattarai P, Dai Z, Chen X. Photothermal therapy and photoacoustic imaging via nanotheranostics in fighting cancer. Chem Soc Rev 2019;48(7):2053-108.

24. Riley RS, Day ES. Gold nanoparticle-mediated photothermal therapy: applications and opportunities for multimodal cancer treatment. Wiley Interdiscip Rev Nanomed Nanobiotechnol. 2017;9(4):e1449.

25. Zhang H, Chen G, Yu B, Cong H. Emerging Advanced Nanomaterials for Cancer Photothermal Therapy. Rev Adv Matter Sci. 2018;53(2):131-46.

26. Hwang S, Nam J, Jung S, Song J, Doh H, Kim S. Gold nanoparticle-mediated photothermal therapy: current status and future perspective. Nanomedicine. 2014;9(13):2003-22.

27. Mitragotri S, Burke PA, Langer R. Overcoming the challenges in administering biopharmaceuticals: formulation and delivery strategies. Nat Rev Drug Discov. 2014;13(9):655-72.

28. Blanco E, Shen H, Ferrari M. Principles of nanoparticle design for overcoming biological barriers to drug delivery. Nat Biotechnol 2015;33(9):941-51.

29. Nakamura Y, Mochida A, Choyke PL, Kobayashi H. Nanodrug Delivery: Is the Enhanced Permeability and Retention Effect Sufficient for Curing Cancer? Bioconjugate Chem. 2016;27(10):2225-38.

30. Matsumoto Y, Nichols JW, Toh K, Nomoto T, Cabral H, Miura Y, et al. Vascular bursts enhance permeability of tumour blood vessels and improve nanoparticle delivery. Nat Nanotechnol. 2016;11(6):533-8.

31. Su Y-L, Hu S-H. Functional Nanoparticles for Tumor Penetration of Therapeutics. Pharmaceutics. 2018;10(4):193.

32. Jain RK, Stylianopoulos T. Delivering nanomedicine to solid tumors. Nat Rev Clin Oncol. 2010;7(11):653-64.

33. Jindal AB. The effect of particle shape on cellular interaction and drug delivery applications of micro- and nanoparticles. Int J Pharm. 2017;532(1):450-65.

34. Li S, Ji Z, Zou M, Nie X, Shi Y, Cheng G. Preparation, characterization, pharmacokinetics and tissue distribution of solid lipid nanoparticles loaded with tetrandrine. AAPS PharmSciTech. 2011;12(3):1011-8.

35. Wang B, He X, Zhang Z, Zhao Y, Feng W. Metabolism of Nanomaterials in Vivo: Blood Circulation and Organ Clearance. Acc Chem Res. 2013;46(3):761-9.

36. Mao Z, Zhou X, Gao C. Influence of structure and properties of colloidal biomaterials on cellular uptake and cell functions. Biomater Sci. 2013;1(9):896-911.

37. Sahay G, Alakhova DY, Kabanov AV. Endocytosis of nanomedicines. J Control Release. 2010;145(3):182-95.

38. Yameen B, Choi WI, Vilos C, Swami A, Shi J, Farokhzad OC. Insight into nanoparticle cellular uptake and intracellular targeting. J Control Release. 2014;190:485-99.

39. Xiao K, Li Y, Luo J, Lee JS, Xiao W, Gonik AM, et al. The effect of surface charge on in vivo biodistribution of PEG-oligocholic acid based micellar nanoparticles. Biomaterials. 2011;32(13):3435-46.

40. Gessner A, Lieske A, Paulke BR, Müller RH. Influence of surface charge density on protein adsorption on polymeric nanoparticles: analysis by two-dimensional electrophoresis. Eur J Pharm Biopharm. 2002;54(2):165-70.

41. Sun T, Zhang YS, Pang B, Hyun DC, Yang M, Xia Y. Engineered Nanoparticles for Drug Delivery in Cancer Therapy. Angew Chem Int Ed Engl 2014;53(46):12320-64.

42. Dias DR, Moreira AF, Correia IJ. The effect of the shape of gold core–mesoporous silica shell nanoparticles on the cellular behavior and tumor spheroid penetration. J Mater Chem B. 2016;4(47):7630-40.

43. Black KCL, Wang Y, Luehmann HP, Cai X, Xing W, Pang B, et al. Radioactive 198Au-doped nanostructures with different shapes for in vivo analyses of their biodistribution, tumor uptake, and intratumoral distribution. ACS Nano. 2014;8(5):4385-94.

44. Toy R, Peiris PM, Ghaghada KB, Karathanasis E. Shaping cancer nanomedicine: the effect of particle shape on the in vivo journey of nanoparticles. Nanomedicine. 2014;9(1):121-34.

45. Doshi N, Prabhakarpandian B, Rea-Ramsey A, Pant K, Sundaram S, Mitragotri S. Flow and adhesion of drug carriers in blood vessels depend on their shape: a study using model synthetic microvascular networks. J Control Release. 2010;146(2):196-200.

46. Thiruppathi R, Mishra S, Ganapathy M, Padmanabhan P, Gulyás B. Nanoparticle Functionalization and Its Potentials for Molecular Imaging. Adv Sci. 2017;4(3):1600279.

47. Corbo C, Molinaro R, Parodi A, Toledano Furman NE, Salvatore F, Tasciotti E. The impact of nanoparticle protein corona on cytotoxicity, immunotoxicity and target drug delivery. Nanomedicine. 2016;11(1):81-100.

48. Palchetti S, Pozzi D, Mahmoudi M, Caracciolo G. Exploitation of nanoparticle–protein corona for emerging therapeutic and diagnostic applications. J Mater Chem B. 2016;4(25):4376-81.

49. Ritz S, Schottler S, Kotman N, Baier G, Musyanovych A, Kuharev J, et al. Protein corona of nanoparticles: distinct proteins regulate the cellular uptake. Biomacromolecules. 2015;16(4):1311-21.

50. Yeo ELL, Thong PSP, Soo KC, Kah JCY. Protein corona in drug delivery for multimodal cancer therapy in vivo. Nanoscale. 2018;10(5):2461-72.

51. Zhao Q, Liu J, Zhu W, Sun C, Di D, Zhang Y, et al. Dual-stimuli responsive hyaluronic acid-conjugated mesoporous silica for targeted delivery to CD44-overexpressing cancer cells. Acta Biomater 2015;23:147-56.

52. Zhou H, Gao Y, Xu H, Li X, Lü Y, Ma T, et al. Hyaluronic Acid-RGD Peptide Conjugated Mesoporous Silica-coated Gold Nanorods for Cancer Dual-targeted Chemo-photothermal Therapy. Journal of Wuhan University of Technology-Mater Sci Ed. 2018;33(2):512-23.

53. Li Z, Yu X-F, Chu PK. Recent advances in cell-mediated nanomaterial delivery systems for photothermal therapy. J Mater Chem B. 2018;6(9):1296-311.

54. Cheng X, Tian X, Wu A, Li J, Tian J, Chong Y, et al. Protein Corona Influences Cellular Uptake of Gold Nanoparticles by Phagocytic and Nonphagocytic Cells in a Size-Dependent Manner. ACS Appl Mater Interfaces. 2015;7(37):20568-75.

55. Richards DA, Maruani A, Chudasama V. Antibody fragments as nanoparticle targeting ligands: a step in the right direction. Chem Sci. 2017;8(1):63-77.

56. Singh P, Pandit S, Mokkapati VRSS, Garg A, Ravikumar V, Mijakovic I. Gold Nanoparticles in Diagnostics and Therapeutics for Human Cancer. Int J Mol Sci. 2018;19(7):1979.

57. Dreaden EC, Alkilany AM, Huang X, Murphy CJ, El-Sayed MA. The golden age: gold nanoparticles for biomedicine. Chem Soc Rev. 2012;41(7):2740-79.

58. Nikoobakht B, El-Sayed MA. Preparation and Growth Mechanism of Gold Nanorods (NRs) Using Seed-Mediated Growth Method. Chem Mater. 2003;15(10):1957-62.

59. Johnson CJ, Dujardin E, Davis SA, Murphy CJ, Mann S. Growth and form of gold nanorods prepared by seed-mediated, surfactant-directed synthesis. J Mater Chem. 2002;12(6):1765-70.

60. Gole A, Murphy CJ. Seed-mediated synthesis of gold nanorods: role of the size and nature of the seed. Chem Mat. 2004;16(19):3633-40.

61. Zhao P, Li N, Astruc D. State of the art in gold nanoparticle synthesis. Coord Chem Rev. 2013;257(3-4):638-65.

62. Liu M, Guyot-Sionnest P. Mechanism of silver (I)-assisted growth of gold nanorods and bipyramids. TJ Phys Chem B. 2005;109(47):22192-200.

63. Pérez-Juste J, Correa-Duarte MA, Liz-Marzán LM. Silica gels with tailored, gold nanorod-driven optical functionalities. Appl Surf Sci 2004;226(1-3):137-43.

64. Kobayashi Y, Correa-Duarte MA, Liz-Marzán LM. Sol− gel processing of silica-coated gold nanoparticles. Langmuir. 2001;17(20):6375-9.

65. Mine E, Yamada A, Kobayashi Y, Konno M, Liz-Marzán LM. Direct coating of gold nanoparticles with silica by a seeded polymerization technique. J Control Release. 2003;264(2):385-90.

66. Moreira AF, Rodrigues CF, Reis CA, Costa EC, Correia IJ. Gold-core silica shell nanoparticles application in imaging and therapy: A review. Microporous Mesoporous Mater. 2018;270:168-79.

67. Zhao N, Yang Z, Li B, Meng J, Shi Z, Li P, et al. RGD-conjugated mesoporous silica-encapsulated gold nanorods enhance the sensitization of triple-negative breast cancer to megavoltage radiation therapy. Int J Nanomedicine. 2016;11:5595-610.

68. Hainfeld J, Slatkin D, Focella T, Smilowitz H. Gold nanoparticles: a new X-ray contrast agent. Br J Radiol. 2006;79(939):248-53.

69. Hou K, Fixler D, Han B, Shi L, Feder I, Duadi H, et al. Towards In Vivo Tumor Detection Using Polarization and Wavelength Characteristics of Self-Assembled Gold Nanorods. Chem Nano Mat. 2017;3(10):736-9.

70. Ashton JR, Castle KD, Qi Y, Kirsch DG, West JL, Badea CT. Dual-Energy CT Imaging of Tumor Liposome Delivery After Gold Nanoparticle-Augmented Radiation Therapy. Theranostics. 2018;8(7):1782-97.

71. Chen Q, Wang H, Liu H, Wen S, Peng C, Shen M, et al. Multifunctional Dendrimer-Entrapped Gold Nanoparticles Modified with RGD Peptide for Targeted Computed Tomography/Magnetic Resonance Dual-Modal Imaging of Tumors. Anal Chem. 2015;87(7):3949-56.

72. Amendola V, Pilot R, Frasconi M, Marago OM, Iati MA. Surface plasmon resonance in gold nanoparticles: a review. J Phys Condens Matter. 2017;29(20):203002.

73. Shajari D, Bahari A, Gill P, Mohseni M. Synthesis and tuning of gold nanorods with surface plasmon resonance. Optical Materials. 2017;64:376-83.

74. Huff TB, Tong L, Zhao Y, Hansen MN, Cheng J-X, Wei A. Hyperthermic effects of gold nanorods on tumor cells. Nanomedicine. 2007;2(1):125-32.

75. Tang F, Li L, Chen D. Mesoporous silica nanoparticles: synthesis, biocompatibility and drug delivery. Adv Mater. 2012;24(12):1504-34.

76. Chen Y-S, Frey W, Kim S, Homan K, Kruizinga P, Sokolov K, et al. Enhanced thermal stability of silica-coated gold nanorods for photoacoustic imaging and image-guided therapy. Optics express. 2010;18(9):8867-78.

77. Pan L, He Q, Liu J, Chen Y, Ma M, Zhang L, et al. Nuclear-targeted drug delivery of TAT peptide-conjugated monodisperse mesoporous silica nanoparticles. J Am Chem Soc. 2012;134(13):5722-5.

78. Alkilany AM, Thompson LB, Boulos SP, Sisco PN, Murphy CJ. Gold nanorods: their potential for photothermal therapeutics and drug delivery, tempered by the complexity of their biological interactions. Adv Drug Delivery Rev. 2012;64(2):190-9.

79. Nel AE, Mädler L, Velegol D, Xia T, Hoek EM, Somasundaran P, et al. Understanding biophysicochemical interactions at the nano–bio interface. Nat Mater. 2009;8(7):543.

80. Walkey CD, Olsen JB, Guo H, Emili A, Chan WC. Nanoparticle size and surface chemistry determine serum protein adsorption and macrophage uptake. J Am Chem Soc. 2012;134(4):2139-47.

81. Lee YK, Choi E-J, Webster TJ, Kim S-H, Khang D. Effect of the protein corona on nanoparticles for modulating cytotoxicity and immunotoxicity. Int J Nanomed. 2015;10(1):97-113.

82. Bertrand N, Grenier P, Mahmoudi M, Lima EM, Appel EA, Dormont F, et al. Mechanistic understanding of in vivo protein corona formation on polymeric nanoparticles and impact on pharmacokinetics. Nat Commun. 2017;8(1):777.

83. Kharazian B, Hadipour NL, Ejtehadi MR. Understanding the nanoparticle-protein corona complexes using computational and experimental methods. Int J Biochem Cell Biol. 2016;75:162-74.

84. Steichen SD, Caldorera-Moore M, Peppas NA. A review of current nanoparticle and targeting moieties for the delivery of cancer therapeutics. Eur J Pharm Sci. 2013;48(3):416-27.

85. Otsuka H, Nagasaki Y, Kataoka K. PEGylated nanoparticles for biological and pharmaceutical applications. Adv Drug Delivery Rev. 2012;55(3):403-19

86. Knop K, Hoogenboom R, Fischer D, Schubert US. Poly (ethylene glycol) in drug delivery: pros and cons as well as potential alternatives. Angew Chem Int Ed. 2010;49(36):6288-308.

87. Kolate A, Baradia D, Patil S, Vhora I, Kore G, Misra A. PEG—a versatile conjugating ligand for drugs and drug delivery systems. J Control Release. 2014;192:67-81.

88. Delgado C, Francis GE, Fisher D. The uses and properties of PEG-linked proteins. Crit Rev Ther Drug Carrier Syst. 1992;9(3-4):249-304.

89. Fang C, Bhattarai N, Sun C, Zhang M. Functionalized nanoparticles with long-term stability in biological media. Small. 2009;5(14):1637-41.

90. Pozzi D, Colapicchioni V, Caracciolo G, Piovesana S, Capriotti AL, Palchetti S, et al. Effect of polyethyleneglycol (PEG) chain length on the bio–nano-interactions between PEGylated lipid nanoparticles and biological fluids: from nanostructure to uptake in cancer cells. Nanoscale. 2014;6(5):2782-92.

91. Owens III DE, Peppas NA. Opsonization, biodistribution, and pharmacokinetics of polymeric nanoparticles. Int J Pharm 2006;307(1):93-102.

92. Suk JS, Xu Q, Kim N, Hanes J, Ensign LM. PEGylation as a strategy for improving nanoparticle-based drug and gene delivery. Adv Drug Delivery Rev. 2016;99((Pt A)):28-51.

93. DeRouchey J, Walker GF, Wagner E, Rädler JO. Decorated rods: a “bottom-up” self-assembly of monomolecular DNA complexes. J Phys Chem B. 2006;110(10):4548-54.

94. Yang Q, Jones SW, Parker CL, Zamboni WC, Bear JE, Lai SK. Evading immune cell uptake and clearance requires PEG grafting at densities substantially exceeding the minimum for brush conformation. Mol Pharm. 2014;11(4):1250-8.

95. Shen S, Tang H, Zhang X, Ren J, Pang Z, Wang D, et al. Targeting mesoporous silica-encapsulated gold nanorods for chemo-photothermal therapy with near-infrared radiation. Biomaterials. 2013;34(12):3150-8.

96. Wang J, Bai R, Yang R, Liu J, Tang J, Liu Y, et al. Size-and surface chemistry-dependent pharmacokinetics and tumor accumulation of engineered gold nanoparticles after intravenous administration. Metallomics. 2015;7(3):516-24.

97. Liu J, Liang H, Li M, Luo Z, Zhang J, Guo X, et al. Tumor acidity activating multifunctional nanoplatform for NIR-mediated multiple enhanced photodynamic and photothermal tumor therapy. Biomaterials. 2018;157:107-24.

98. Ishida T, Atobe K, Wang X, Kiwada H. Accelerated blood clearance of PEGylated liposomes upon repeated injections: effect of doxorubicin-encapsulation and high-dose first injection. J Control Release. 2006;115(3):251-8.

99. Lila ASA, Kiwada H, Ishida T. The accelerated blood clearance (ABC) phenomenon: clinical challenge and approaches to manage. J Control Release. 2013;172(1):38-47.

100. Konradi R, Pidhatika B, Mühlebach A, Textor M. Poly-2-methyl-2-oxazoline: a peptide-like polymer for protein-repellent surfaces. Langmuir. 2008;24(3):613-6.

101. Mero A, Pasut G, Dalla Via L, Fijten MW, Schubert US, Hoogenboom R, et al. Synthesis and characterization of poly (2-ethyl 2-oxazoline)-conjugates with proteins and drugs: suitable alternatives to PEG-conjugates? J Control Release. 2008;125(2):87-95.

102. Koshkina O, Westmeier D, Lang T, Bantz C, Hahlbrock A, Würth C, et al. Tuning the Surface of Nanoparticles: Impact of Poly (2-ethyl-2-oxazoline) on Protein Adsorption in Serum and Cellular Uptake. Macromol Biosci. 2016;16(9):1287-300.

103. Moreira AF, Rodrigues CF, Reis CA, Costa EC, Ferreira P, Correia IJ. Development of poly-2-ethyl-2-oxazoline coated gold-core silica shell nanorods for cancer chemo-photothermal therapy. Nanomedicine. 2018;13(20):2611-27.

104. Li Y, Hu H, Zhou Q, Ao Y, Xiao C, Wan J, et al. α-Amylase-and Redox-Responsive Nanoparticles for Tumor-Targeted Drug Delivery. ACS Appl Mater Interfaces. 2017;9(22):19215-30.

105. Moreira AF, Dias DR, Costa EC, Correia IJ. Thermo-and pH-responsive nano-in-micro particles for combinatorial drug delivery to cancer cells. Eur J Pharm Sci 2017;104:42-51.

106. Zhang C, Pan D, Li J, Hu J, Bains A, Guys N, et al. Enzyme-responsive peptide dendrimer-gemcitabine conjugate as a controlled-release drug delivery vehicle with enhanced antitumor efficacy. Acta Biomater. 2017;55:153-62.

107. Li H, Tan L-L, Jia P, Li Q-L, Sun Y-L, Zhang J, et al. Near-infrared light-responsive supramolecular nanovalve based on mesoporous silica-coated gold nanorods. Chem Sci 2014;5(7):2804-8.

108. Liu J, Detrembleur C, De Pauw-Gillet MC, Mornet S, Jérôme C, Duguet E. Gold Nanorods Coated with Mesoporous Silica Shell as Drug Delivery System for Remote Near Infrared Light-Activated Release and Potential Phototherapy. Small. 2015;11(19):2323-32.

109. Tang H, Shen S, Guo J, Chang B, Jiang X, Yang W. Gold nanorods@mSiO2 with a smart polymer shell responsive to heat/near-infrared light for chemo-photothermal therapy. J Mater Chem. 2012;22(31):16095-103.

110. Lee ES, Gao Z, Bae YH. Recent progress in tumor pH targeting nanotechnology. J Control Release. 2008;132(3):164-70.

111. Du J, Lane LA, Nie S. Stimuli-responsive nanoparticles for targeting the tumor microenvironment. J Control Release. 2015;219:205-14.

112. Vander Heiden MG, Cantley LC, Thompson CB. Understanding the Warburg effect: the metabolic requirements of cell proliferation. Science. 2009;324(5930):1029-33.

113. Zhang T, Ding Z, Lin H, Cui L, Yang C, Li X, et al. pH-Sensitive Gold Nanorods with a Mesoporous Silica Shell for Drug Release and Photothermal Therapy. Eur J Pharm Sci 2015;2015(13):2277-84.

114. Zeiderman MR, Morgan DE, Christein JD, Grizzle WE, McMasters KM, McNally LR. Acidic pH-targeted chitosan-capped mesoporous silica coated gold nanorods facilitate detection of pancreatic tumors via multispectral optoacoustic tomography. ACS Biomater Sci Eng. 2016;2(7):1108-20.

115. Zhang Z, Liu C, Bai J, Wu C, Xiao Y, Li Y, et al. Silver nanoparticle gated, mesoporous silica coated gold nanorods (AuNR@ MS@ AgNPs): low premature release and multifunctional cancer theranostic platform. ACS Appl Mater Interfaces. 2015;7(11):6211-9.

116. Zhang Z, Wang J, Nie X, Wen T, Ji Y, Wu X, et al. Near infrared laser-induced targeted cancer therapy using thermoresponsive polymer encapsulated gold nanorods. J Am Chem Soc. 2014;136(20):7317-26.

117. Baek S, Singh RK, Kim T-H, Seo J-w, Shin US, Chrzanowski W, et al. Triple hit with drug carriers: pH-and temperature-responsive theranostics for multimodal chemo-and photothermal therapy and diagnostic applications. ACS Appl Mater Interfaces. 2016;8(14):8967-79.

118. An N, Lin H, Qu F. Synthesis of a GNRs@ mSiO2-ICG-DOX@ Se-Se-FA Nanocomposite for Controlled Chemo-/Photothermal/Photodynamic Therapy. Eur J Pharm Sci 2018;2018(39):4375-84.

119. Fang J, Nakamura H, Maeda H. The EPR effect: unique features of tumor blood vessels for drug delivery, factors involved, and limitations and augmentation of the effect. Adv Drug Delivery Rev. 2011;63(3):136-51.

120. Matsumoto Y, Nichols JW, Toh K, Nomoto T, Cabral H, Miura Y, et al. Vascular bursts enhance permeability of tumour blood vessels and improve nanoparticle delivery. Nat Nanotechnol. 2016;11(6):533.

121. Shi J, Kantoff PW, Wooster R, Farokhzad OC. Cancer nanomedicine: progress, challenges and opportunities. Nat Rev Cancer. 2017;17(1):20.

122. Maeda H, Wu J, Sawa T, Matsumura Y, Hori K. Tumor vascular permeability and the EPR effect in macromolecular therapeutics: a review. J Control Release. 2000;65(1-2):271-84.

123. Danhier F. To exploit the tumor microenvironment: since the EPR effect fails in the clinic, what is the future of nanomedicine? J Control Release. 2016;244:108-21.

124. Wilhelm S, Tavares AJ, Dai Q, Ohta S, Audet J, Dvorak HF, et al. Analysis of nanoparticle delivery to tumours. Nat Rev Mater. 2016;1(5):16014.

125. Huang P, Bao L, Zhang C, Lin J, Luo T, Yang D, et al. Folic acid-conjugated silica-modified gold nanorods for X-ray/CT imaging-guided dual-mode radiation and photo-thermal therapy. Biomaterials. 2011;32(36):9796-809.

126. Luo GF, Chen WH, Lei Q, Qiu WX, Liu YX, Cheng YJ, et al. A Triple-Collaborative Strategy for High-Performance Tumor Therapy by Multifunctional Mesoporous Silica-Coated Gold Nanorods. Adv Funct Mater. 2016;26(24):4339-50.

127. Andreev OA, Engelman DM, Reshetnyak YK. Targeting acidic diseased tissue: New technology based on use of the pH (Low) Insertion Peptide (pHLIP). Chimica oggi. 2009;27(2):34.

128. Hemmer E, Benayas A, Légaré F, Vetrone F. Exploiting the biological windows: current perspectives on fluorescent bioprobes emitting above 1000 nm. Nanoscale Horiz. 2016;1(3):168-84.

129. Xia H-X, Yang X-Q, Song J-T, Chen J, Zhang M-Z, Yan D-M, et al. Folic acid-conjugated silica-coated gold nanorods and quantum dots for dual-modality CT and fluorescence imaging and photothermal therapy. J Mater Chem B. 2014;2(14):1945-53.

130. Lee C, Hwang HS, Lee S, Kim B, Kim JO, Oh KT, et al. Rabies Virus-Inspired Silica-Coated Gold Nanorods as a Photothermal Therapeutic Platform for Treating Brain Tumors. Adv Mater. 2017;29(13):1605563.

131. Terentyuk G, Panfilova E, Khanadeev V, Chumakov D, Genina E, Bashkatov A, et al. Gold nanorods with a hematoporphyrin-loaded silica shell for dual-modality photodynamic and photothermal treatment of tumors in vivo. Nano Res. 2014;7(3):325-37.

132. Monem AS, Elbialy N, Mohamed N. Mesoporous silica coated gold nanorods loaded doxorubicin for combined chemo–photothermal therapy. Int J Pharm. 2014;470(1-2):1-7.

133. Gorelikov I, Matsuura N. Single-Step Coating of Mesoporous Silica on Cetyltrimethyl Ammonium Bromide-Capped Nanoparticles. Nano Lett. 2008;8(1):369-73.

134. Moreira AF, Gaspar VM, Costa EC, de Melo-Diogo D, Machado P, Paquete CM, et al. Preparation of end-capped pH-sensitive mesoporous silica nanocarriers for on-demand drug delivery. Eur J Pharm Sci. 2014;88(3):1012-25.

135. Rodrigues CF, Reis CA, Moreira AF, Ferreira P, Correia IJ. Optimization of gold core-mesoporous silica shell functionalization with TPGS and PEI for cancer therapy. Microporous Mesoporous Mater. 2019;285:1-12.

136. Yildirim A, Ozgur E, Bayindir M. Impact of mesoporous silica nanoparticle surface functionality on hemolytic activity, thrombogenicity and non-specific protein adsorption. J Mater Chem B,. 2013;1(14):1909-20.

137. Reis CA, Rodrigues CF, Moreira AF, Jacinto TA, Ferreira P, Correia IJ. Development of gold-core silica shell nanospheres coated with poly-2-ethyl-oxazoline and ß-cyclodextrin aimed for cancer therapy. Mater Sci Eng C Mater Biol Appl 2019;98:960-8.

138. Bernd A, Ott M, Ishikawa H, Schroten H, Schwerk C, Fricker G. Characterization of efflux transport proteins of the human choroid plexus papilloma cell line HIBCPP, a functional in vitro model of the blood-cerebrospinal fluid barrier. Pharm Res. 2015;32(9):2973-82.

139. Gaspar VM, Moreira AF, Costa EC, Queiroz JA, Sousa F, Pichon C, et al. Gas-generating TPGS-PLGA microspheres loaded with nanoparticles (NIMPS) for co-delivery of minicircle DNA and anti-tumoral drugs. Colloids and surfaces B, Biointerfaces. 2015;134:287-94.

140. Kim JH, Moon MJ, Kim DY, Heo SH, Jeong YY. Hyaluronic Acid-Based Nanomaterials for Cancer Therapy. Polymers. 2018;10(10):1133.

141. Lokeshwar VB, Mirza S, Jordan A. Targeting hyaluronic acid family for cancer chemoprevention and therapy. Adv Cancer Res. 2014;123:35-65.

142. Yang C, He Y, Zhang H, Liu Y, Wang W, Du Y, et al. Selective killing of breast cancer cells expressing activated CD44 using CD44 ligand-coated nanoparticles in vitro and in vivo. Oncotarget. 2015;6(17):15283-96.

143. Yang C, Wu T, Qi Y, Zhang Z. Recent Advances in the Application of Vitamin E TPGS for Drug Delivery. Theranostics. 2018;8(2):464-85.

144. Yan B, Qiao X-F. Rare-Earth/Inorganic/Organic Polymeric Hybrid Materials: Molecular Assembly, Regular Microstructure and Photoluminescence. J Phys Chem B. 2007;111(43):12362-74.

145. Wu Y, Chu Q, Tan S, Zhuang X, Bao Y, Wu T, et al. D-alpha-tocopherol polyethylene glycol succinate-based derivative nanoparticles as a novel carrier for paclitaxel delivery. Int J Nanomedicine. 2015;10(1):5219-35.

146. Yu M, Jambhrunkar S, Thorn P, Chen J, Gu W, Yu C. Hyaluronic acid modified mesoporous silica nanoparticles for targeted drug delivery to CD44-overexpressing cancer cells. Nanoscale. 2013;5(1):178-83.

147. Maiz-Fernandez S, Perez-Alvarez L, Ruiz-Rubio L, Perez Gonzalez R, Saez-Martinez V, Ruiz Perez J, et al. Synthesis and Characterization of Covalently Crosslinked pH-Responsive Hyaluronic Acid Nanogels: Effect of Synthesis Parameters. Polymers 2019;11(4):742.

148. Becker J, Trügler A, Jakab A, Hohenester U, Sönnichsen C. The Optimal Aspect Ratio of Gold Nanorods for Plasmonic Bio-sensing. Plasmonics. 2010;5(2):161-7.

149. He T, Jańczewski D, Jana S, Parthiban A, Guo S, Zhu X, et al. Efficient and robust coatings using poly(2-methyl-2-oxazoline) and its copolymers for marine and bacterial fouling prevention. J Polym Sci, Part A: Polym Chem. 2016;54(2):275-83.

150. Ernsting MJ, Murakami M, Roy A, Li SD. Factors controlling the pharmacokinetics, biodistribution and intratumoral penetration of nanoparticles. J Control Release. 2013;172(3):782-94.

151. Cui X, Cheng W, Han X. Lipid bilayer modified gold nanorod@mesoporous silica nanoparticles for controlled drug delivery triggered by near-infrared light. J Mater Chem B. 2018;6(48):8078-84.

152. Mangalathillam S, Rejinold NS, Nair A, Lakshmanan V-K, Nair SV, Jayakumar R. Curcumin loaded chitin nanogels for skin cancer treatment via the transdermal route. Nanoscale. 2012;4(1):239-50.

153. Li C, Jin J, Liu J, Xu X, Yin J. Stimuli-Responsive Polypropylene for the Sustained Delivery of TPGS and Interaction with Erythrocytes. ACS Appl Mater Interfaces. 2014;6(16):13956-67.

154. Alves CG, de Melo-Diogo D, Lima-Sousa R, Costa EC, Correia IJ. Hyaluronic acid functionalized nanoparticles loaded with IR780 and DOX for cancer chemo-photothermal therapy. Eur J Pharm Biopharm 2019;137:86-94.

155. Liao J, Zheng H, Fei Z, Lu B, Zheng H, Li D, et al. Tumor-targeting and pH-responsive nanoparticles from hyaluronic acid for the enhanced delivery of doxorubicin. Int J Biol Macromol. 2018;113:737-47.

156. de Melo-Diogo D, Pais-Silva C, Dias DR, Moreira AF, Correia IJ. Strategies to Improve Cancer Photothermal Therapy Mediated by Nanomaterials. Adv Healthc Mater. 2017;6(10):1700073.